MARTIAN PALEOMAGNETISM WITH THE SQUID MICROSCOPE

Thesis by

Benjamin Paul Weiss

In Partial Fulfillment of the Requirements for the

Degree of

Doctor of Philosophy

CALIFORNIA INSTITUTE OF TECHNOLOGY

Pasadena, California

2003

(Defended January 28, 2003)

ACKNOWLEDGEMENTS

There are of course many people who need to be thanked for making this thesis possible, but by far the most important of these is Joe Kirschvink. Joe couldn't have had me in his lab more than a week before trusting me and a fellow undergraduate—the two of us new to geology, unproven and truly nobodies—to stay up all night slicing up the martian meteorite ALH84001. All night long we kept laughing out of excitement and disbelief as we played with not only an invaluable rock from Mars but the oldest known rock from any planet! This ability to inspire through his trust is Joe's genius as a teacher. Joe also taught me how to be at once fearlessly creative and within the bounds of rigor. To me, it is the stories—of the rocks, of the events of the past, and of how we learn about them—that were what attracted me to planetary science in the first place. Trucking around the world with Joe (through South Africa, Swaziland, Mexico, Australia, Japan…), I saw some really strange rocks and places, which had even stranger stories to tell. Strange, at least, when told through Joe as their interpreter (Joe says I am a Martian that has just recently taken over a human body but hasn't quite learned how to use all of the equipment; if this is true, then where did *he* come from?). As I hope this thesis shows, Joe has taught me how to tell some really interesting stories myself, a gift for which I am in his debt.

Many other people contributed to my education. My parents supported my adventures in astronomy in school and at summer camp for many years; without their early confidence in me, I would be nowhere today. Franz Baudenbacher has generously shared with me his extraordinary instrument, the SQUID Microscope, which played a critical role in many of the discoveries described here. Tanja Bosak has been my most persistent critic, friend and companion.

The work presented here is the result of a collaborative effort with many people:

Chapter 1: This article was co-written with Franz Baudenbacher, John Wikswo, and Joe Kirschvink. The development of the Vanderbilt LTS SQUID microscopes has been funded in part by grants from the National Science Foundation and the National Institutes of Health. We thank W. Goree for valuable discussions.

Chapter 2: This article was co-written with Franz Baudenbacher, John Wikswo, and Joe Kirschvink, Nick Peters, Francis MacDonald, and Hojatollah Vali. We are grateful, for support and samples, to the NASA Ancient Martian Meteorite program, the NASA Astrobiology Institute, the NASA Cosmochemistry program, the Division of Biological Infrastructure of the NSF, and the NIH. Financial support to H.V. was provided by the Natural Sciences and Engineering Research Council of Canada. We also thank A. Treiman, A. Maine, and S. Stewart for stimulating discussions, G. Rossman for thoughtful advice and use of equipment, and M. Sankaran and J. Maurer for help with the low-temperature experiments.

Chapter 3: This article was co-written with Hojatollah Vali, Franz Baudenbacher, Joe Kirschvink, Sarah Stewart, and David Shuster. We thank V. Courtillot, D.J. Stevenson, M. Purucker, M.T. Zuber, and L. Hedges for encouragement and thoughtful advice, D. Mann of High Mesa Petrographics for producing unheated thin sections, T. Kamino of Hitachi Japan for assistance with the FIB and FEG-TEM, K. Thomas-Keprta for providing data for Fig. 3.5, and T. Puig for valuable logistical help. Financial support for B.P.W. and J.L.K. was provided by the NASA Exobiology program and the NASA Astrobiology Institute. Financial support to H.V. was provided by National Science and Engineering Research Council of Canada (NSERC).

Chapter 4: This article was co-written with David Shuster and Sarah Stewart. We thank K. Farley for providing the code for his (U-Th)/He thermochronology program and D. Bogard for supplying the raw Ar/Ar data used by this study. We also thank J. Kirschvink, V. Courtillot, D. Bogard, S. Mukhopadhyay, K. Farley, and B. Murray for helpful discussions and encouragement. Financial support for B.P.W. was provided by the NASA Exobiology Program and the NASA Astrobiology Institute. D.L.S. is supported by a National Science Foundation Graduate Research Fellowship.

With Joe at Shark Bay, Australia, July 2001

ABSTRACT

Rocks should preserve natural remanent magnetizations with stable directional and intensity information at levels ~1000 times below that of the noise level on today's best moment magnetometers. The superconducting quantum interference device (SQUID) Microscope is a new, high-resolution magnetometer that can now detect such weak signals. It maps the magnetic fields above samples with a spatial resolution of <100 μm and a moment sensitivity of $<10^{-15}$ Am^2. It therefore provides data with a resolution directly comparable with that of other common petrographic techniques. This thesis describes applications of SQUID microscopy to a variety of problems in the planetary sciences.

A SQUID microscope paleomagnetic conglomerate test demonstrates that ALH84001 has been cooler than ~40°C since before its ejection from the surface of Mars at 15 Ma. Because this temperature cannot sterilize most bacteria or eukarya, these data support the hypothesis that meteorites could transfer life between planets in the solar system. These and other data on panspermia demand a re-evaluation of the long-held assumption that terrestrial life evolved in isolation on Earth.

Subsequent magnetic and textural studies of the meteorite show that 4 Ga ALH84001 carbonates containing magnetite and pyrrhotite carry a stable natural remanent magnetization. $^{40}Ar/^{39}Ar$ thermochronology demonstrates that this magnetization originated at 3.9-4.1 Ga on Mars. This magnetization is the oldest known for a planetary rock, and its strong intensity suggests that Mars had generated a geodynamo at or before 4 Ga. The intensity of the field that magnetized ALH84001 was roughly within an order of magnitude of that at the surface of the present-day Earth, sufficient for magnetotaxis by the

bacteria whose magnetofossils have been reported in ALH84001 and possibly for the production of the strong crustal anomalies.

$^{40}Ar/^{39}Ar$ thermochronology calculations also provide an explanation for why ALH84001 contains a sample of an apparently ancient martian atmosphere. Because this gas is enriched in light isotopes of H and N relative to that on present-day Mars, this supports the hypothesis that the planet has experienced significant atmospheric loss since 4 Ga. These calculations also suggest that for the last 4 Gyr, average surface temperatures on Mars may not have been much higher than the present cold conditions.

TABLE OF CONTENTS

LIST OF ILLUSTRATIONS AND TABLES

Table *Page*

Chapter 1

SQUID MICROSCOPY: A NEW TOOL FOR PALEOMAGNETISM[1]

Twenty years ago, Kirschvink [1] argued that many paleomagnetic studies were limited by the sensitivity of the magnetometer systems then in use. He showed that sedimentary rocks could preserve stable, detrital remanent magnetizations at levels of 10^{-14} to 10^{-15} Am^2, about 100 to 1000 times below the noise level of today's best superconducting quantum interference device (SQUID) rock magnetometers. If a more sensitive magnetometer could be built, it would dramatically expand the range and variety of rock types amenable to paleomagnetic analysis. Just such an instrument is now on the horizon: the low-temperature superconductivity (LTS) SQUID Microscope.

The LTS SQUID Microscope is the end-product of more than a decade of work on the application of high-resolution SQUID magnetometers to cardiology research by Franz Baudenbacher and John Wikswo of Vanderbilt University [2-4]. Its current prototype, the Ultra High Resolution Scanning SQUID Microscope (UHRSSM), maps the vertical component of the magnetic field above the surface of a sample at room temperature and pressure. It can achieve this with a spatial resolution of <100 μm and a moment sensitivity (i.e., minimum detectable dipole moment) 10,000 times that of the most recent 2G Enterprises® Superconducting Rock Magnetometer (2G® SRM). The art of LTS SQUID microscopy has now progressed to the point that the fields of samples placed within the vacuum region of some instruments can be measured with spatial

[1] Adapted from: Weiss, B. P., F. J. Baudenbacher, J. P. Wikswo, and J. L. Kirschvink (2001) Magnetic microscopy promises a leap in sensitivity and resolution, *Eos Trans. AGU*, **82**, 513 & 518.

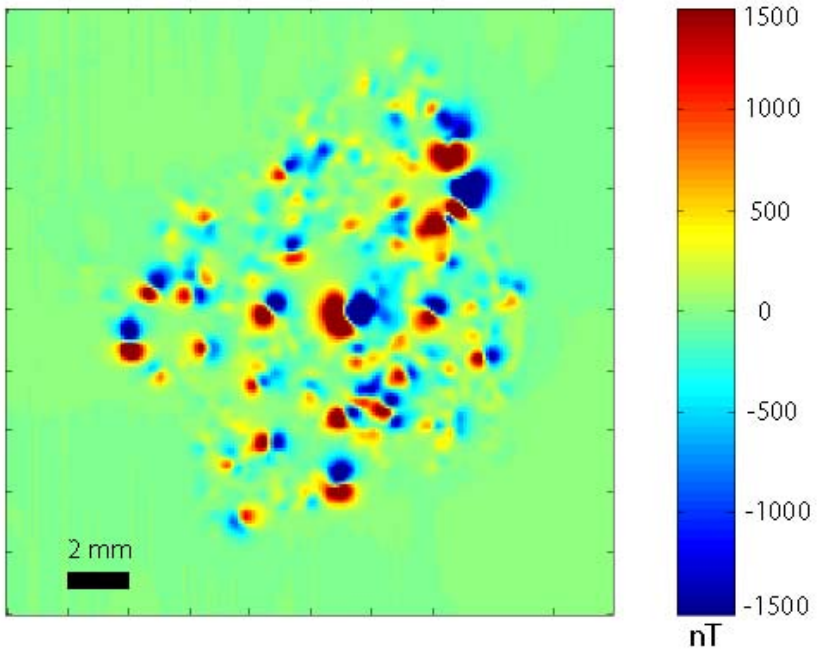

Fig. 1.1 Ultra High Resolution Scanning SQUID Microscope (UHRSSM) image of type CR2 carbonaceous chondrite GRA95229. Shown is the intensity of the out-of-the-page component of the magnetic field as observed ~100 μm above a 30-μm thin section of the meteorite. Numerous, randomly oriented dipolar features associated with chondrules and matrix are visible. The prototype SQUID microscope which made this image has a spatial resolution of 250 μm. Sample courtesy of H. Connolly.

resolutions of only several micrometers.

Although magnetic force microscopes (MFMs) have better moment sensitivities than SQUID microscopes, the current generation of SQUID microscopes have field sensitivities 100,000 times better than MFMs and do not suffer from the sample-instrument interactions that plague MFM-sensing of magnetically soft materials. These interactions make MFMs difficult to use for quantitative measurements of the magnetic field above samples. Although it has ~10,000 times lower spatial resolution than a typical MFM, the UHRSSM quantitatively maps the magnetic fields of rock slices and thin sections at spatial resolutions 10-

100 times better than that of the best existing SQUID rock magnetometers. It can therefore provide data with a resolution comparable to that of other common petrographic techniques such as optical and electron microscopy (Fig. 1.1). This bridges the roughly six-orders-of-magnitude gap in spatial resolution between 2G® SRMs and MFMs, such that magnetization can be directly correlated with distinct minerals and textures.

Both the UHRSSM and 2G® SRM use similar commercially available DC-SQUIDs operating at or near their thermal noise limits. So how can the SQUID microscope achieve such superior sensitivity at such high spatial resolution? Much of the answer lies in the closed geometry of dipolar magnetic fields and how their detection depends upon instrument size.

First, consider the 2G® 760 SRM (Fig. 1.2a). A room-temperature sample is inserted into the middle of several ~8 cm diameter Helmholtz-style pickup coils held at 4 K. The large temperature difference between the sample and the coil requires shielding the coils within a dewar, heat-sunk radiation baffles, and many layers of superinsulation. Because they need to encircle both these structures and the sample, the coils need to be rather large in size. Although large coils are better for detecting uniform magnetic fields, they are less sensitive to dipoles than are small coils because they encompass more of the sample's fringing fields oriented in the opposite sense to its magnetization (Fig. 1.2a). The result is a Catch-22: once the geometry of the system is set by the coil diameter and the room-temperature access, the samples should be made as large as possible to achieve the optimum signal-to-noise ratio. This reduces the effective spatial resolution of the system (which is set by the diameter of the coils) and means that the sensitivity to small samples is far from optimum.

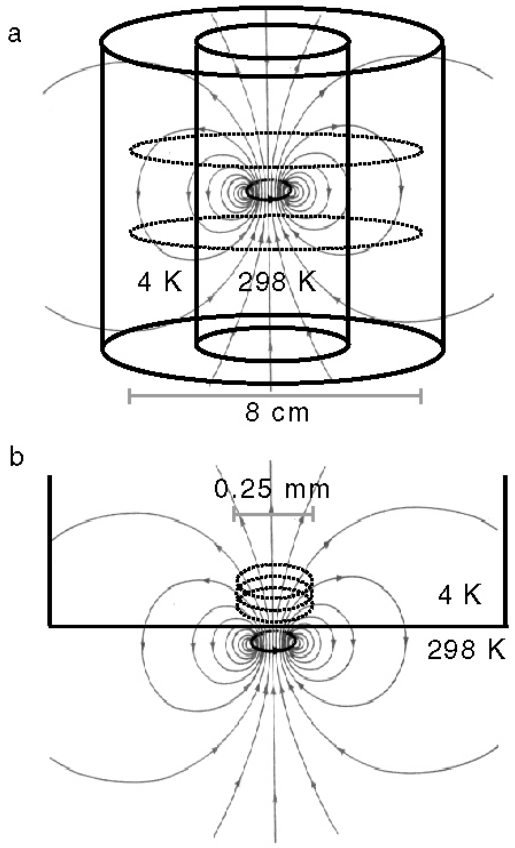

Fig. 1.2 Comparison of the SQUID Microscope with a standard moment magnetometer. **a)** Schematic cross section of a 2G Enterprises® Superconducting Rock Magnetometer, showing pair of Helmholtz coils (dashed) held at 4 K and enclosed by shielding. A room temperature sample with a dipolar magnetization oriented upwards, represented as a current loop, is at the center of the coils. The large coils (~8 cm diameter) encompass much of the downward, fringing fields. **b)** Schematic cross section of sensing region of the SQUID Microscope, showing pickup coil (dashed) held at 4 K, separated from the same sample by a thin (30 μm) sapphire window. The smaller coil (250 μm diameter) encompasses less of the downward, fringing fields. Both diagrams are not to scale.

Now, consider the UHRSSM (Fig. 1.2b). The major difference is that its pickup coil does not encircle the sample but instead is brought very close, within 100 μm. This is not an easy task, because the 250 μm diameter, 4 K coil is only separated from the room-temperature environment by a 30 μm thick sapphire window, such that the temperature gradient from coil to sample is several million ºC/m! Nevertheless, because the coil is so small, the cryogenic surface area that

is exposed to room-temperature thermal radiation is quite small. Thus, the thermal loads on the system are rather modest. The engineering feat of getting a 4 K SQUID to operate within 100 μm of a room-temperature rock eliminates the requirement that the coil encircle the sample, such that much less of the fringing field is encompassed (Fig. 1.2b).

Although the field sensitivity of the coil decreases as the coil is made smaller, the magnetic field produced by the dipole increases as $1/r^3$ for distance r between the dipole and coil. If the coil with radius a is at a height a above the sample—which optimizes the tradeoff between sensitivity and spatial resolution—it is easy to show that for a uniformly magnetized sample much smaller than a, the signal-to-noise ratio scales as roughly $1/a$. A smaller coil brought closer to the sample produces higher sensitivity measurements.

Now, if the coil diameter a is larger than the sample-to-coil distance r (as is the case for the UHRSSM and 2G® SRM), then the spatial resolution of the magnetometer is limited by the coil size. Thus, the dramatic increase in sensitivity resulting from the small size of the coil is accompanied by high spatial resolution. This may seem counter intuitive, because for many laboratory instruments—for instance, spectrometers, or microscopes—spatial resolution and sensitivity are often negatively correlated. But for the imaging of magnetic dipoles, the inverse relationship between sensitivity and coil size in SQUID microscopy persists as long as the coil (and coil-to-sample distance) remain larger than the size of the magnetized region that is being targeted.

The chief limitation of SQUID microscopy comes from the problem of inverting the data output—a spatial grid of vertical components of the magnetic field—into a three-dimensional vector magnetization pattern within the sample, the quantity usually desired by paleomagnetists. This problem is identical to that encountered in the inversion of aeromagnetic field data to a map of lithospheric

magnetization. A similar problem is also encountered by those using MFMs and 2G® SRMs, which measure the spatial derivative of the magnetic force field and net magnetization vector, respectively, of the sample. None of these instruments directly measures the spatially heterogeneous magnetization pattern within the target. All suffer from the difficulty that without other constraints, there is no unique magnetization pattern that can be derived from measurements of the magnetic field taken outside the magnetized region.

In practice, this usually does not mean that the inversion is intractable, because many magnetization patterns can be ruled out from other constraints. For instance, only certain magnetization intensities will be plausible given compositional constraints from electron microscopy, microprobe, and other techniques. Scanning electron microscopy and other textural data can be used to localize the boundaries of discrete grains, which are often unidirectionally magnetized, to further reduce the solution space. Also, magnetizations with high amplitudes and spatial frequencies can often be rejected. One can require that the magnetization solution have minimum norm and maximum smoothness. Measurements of all three components of the net magnetization of the sample with a 2G® SRM will further constrain the solution.

Certain more general criteria can also be required of the magnetization solution. For instance, one can assume that the solution is composed of a grid of finite number of regularly spaced fixed-location dipoles whose intensity and direction are allowed to vary (an "equivalent source" scheme). For samples with a modest number of discrete magnetized grains, the use of a three-axis SQUID microscope, which is currently in development, may also help alleviate the inverse problem.

Initial collaborative work between the Caltech paleomagnetism and Vanderbilt SQUID groups on 1 mm thick slices and 30 μm thin sections of martian

meteorite ALH84001 [5-7] (see Chapters 2-4) has already demonstrated that SQUID microscopy will enable a whole new class of paleomagnetic analyses. Conglomerate, baked contact, and fold tests can be performed on extremely small spatial scales, vastly expanding the utility of these critical geological field tests of magnetic stability. A suite of rock-magnetic and paleomagnetic experiments can be done on individual grains in standard petrographic thin sections at very high rates, allowing the observed magnetic components to be matched with the minerals that are present. This is only the beginning. An improvement in instrumental sensitivity by only a factor of a few—like the magnificent Keck Telescopes, each with a collecting area four times that of the Hale Telescope—-is usually considered a major advance that opens new research opportunities. A sudden increase in measuring technique by four orders of magnitude, accompanied by a one to two order-of-magnitude increase in spatial resolution, could be a revolution for paleomagnetism and rock magnetism.

We are currently developing a second-generation LTS SQUID microscope to be located in the magnetically shielded clean laboratory at Caltech. Funds are being sought to make this new instrument open for use by the general paleomagnetic community, and within a few years these instruments should become commercially available.

Chapter 2

A LOW TEMPERATURE TRANSFER OF ALH84001 FROM MARS TO EARTH[2]

The ejection of material from Mars is thought to be caused by large impacts that would heat much of the ejecta to high temperatures. Images of the magnetic field of martian meteorite ALH84001 reveal a spatially heterogeneous pattern of magnetization associated with fractures and rock fragments. A paleomagnetic conglomerate test and petrographic data indicate that the interior of the rock has probably not been above even 40°C since before its ejection from the surface of Mars at 15 Ma. Because these temperatures cannot sterilize most bacteria or eukarya, these data support the hypothesis that meteorites could transfer life between planets in the solar system.

1. Introduction

Large-body impacts are the only known natural processes capable of ejecting a rock from Mars. It has been suggested that some rocks could be ejected without being shocked and heated [8, 9], and laboratory shock experiments have spalled lightly shocked material moving at about 20% of Mars' escape velocity [10]. Thermal conductivity calculations [11] demonstrate that passage through Earth's

[2] Adapted from: Weiss, B. P., J. L. Kirschvink, F. J. Baudenbacher, H. Vali, N. T. Peters, F. A. Macdonald, and J. P. Wikswo (2000) A low temperature transfer of ALH84001 from Mars to Earth, *Science*, **290**, 791-795.

present atmosphere will not heat the centers of meteorites larger than ~0.3 cm above 100°C.

ALH84001 is a meteorite composed of ~95% orthopyroxene that accumulated in a magma chamber on Mars ~4.5 billion years ago (Ga) [12]. Carbonate blebs, which may contain evidence for ancient life on Mars [13], formed in its fractures at about 4 Ga [14]. During its first few billion years, ALH84001 experienced several shocks, probably from minor planet impacts [15]. It was launched from the surface of Mars ~15 million years ago by another impact [16] and after wandering through space [17], landed in Antarctica about 11 thousand years ago (ka).

Kirschvink *et al.* [18] suggested that the interior of ALH84001 has been cooler than 110°C since before the formation of the carbonate. To obtain more precise thermal constraints on the ejection of ALH84001 from Mars, we applied a low-blocking temperature conglomerate test to the meteorite. Magnetic measurements were conducted using SQUID microscopy, a new technique for making high-resolution maps of sample magnetic fields.

2. Ferromagnetic Mineralogy of ALH84001

Our transmission electron microscopy imaging of the rims of the carbonate blebs in an ultrathin section prepared by focused ion beam detected single domain (SD) and superparamagnetic (SP) magnetite (Fe_3O_4) and monoclinic pyrrhotite (Fe_7S_8) with characteristic lattice fringes (see Chapter 3 and Figs. 3.2 and 3.3). Because magnetic minerals have not been positively identified outside the carbonate bleb's rims, the blebs probably carry most of the magnetization in ALH84001 (for a confirmation of this conclusion, see Chapter 3). Other studies [19] have shown

that this magnetite is stoichiometric (impurities <0.1%). After exposure to a 5-T field at room temperature, a 20 mg pyroxenite grain from ALH84001,236 containing multiple carbonate blebs exhibited a remanence transition at ~112 K and another possible transition at ~35 K, diagnostic of low-Ti magnetite ($Fe_{3-z}Ti_zO4$ with $z \approx 0.01$) and pyrrhotite, respectively (Fig. 2.1). The grain's magnetization increased during cooling and then recovered ~90% of its original magnetization upon warming to room temperature, indicating the presence of SP and SD crystals and a lack of multidomain (MD) crystals. Anhysteretic remanent magnetization (ARM) and isothermal remanent magnetization (IRM) acquisition and demagnetization experiments on this grain also provide evidence of pyrrhotite (it acquires an IRM up to and beyond 1000 mT) and a small fraction of pseudo–single domain (PSD) crystals (alternating-field demagnetization is more effective at removing an IRM than an ARM). X-ray maps obtained by electron microprobe analysis detected Fe-sulfide crystals dispersed through the pyroxene matrix, suggesting that pyrrhotite may also be present outside the carbonate. We have thus detected two major magnetic minerals in ALH84001, located in the carbonate blebs and also probably in the pyroxene: magnetite and pyrrhotite ranging in size between SP, SD, and PSD. This confirms a previous identification of these magnetic minerals [18] and argues against the presence of titanomagnetite [20].

3. Paleomagnetic Methods

Eight oriented slices of ALH84001 were analyzed for this study. The eight slices were oriented using the fine sawblade striations left on the original flat surface cut at the Johnson Space Center (Houston, TX) during the sampling of the meteorite. In a class-1000 magnetically shielded clean lab at the California Institute of Technology (Caltech), the oriented fragments were cemented onto

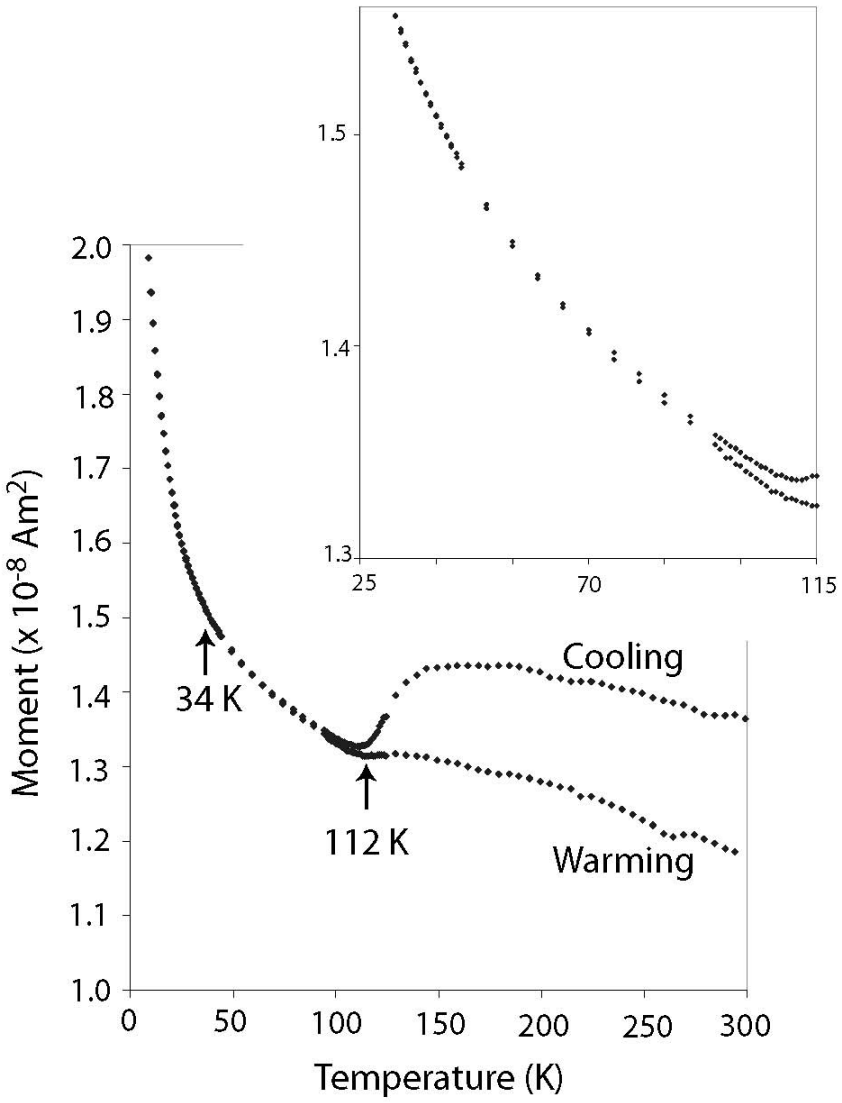

Fig. 2.1 Low-temperature cycling of ALH84001,236. Shown is the moment of the ~20-mg pyroxenite grain in a quenched ($<2\times10^{-4}$ T) field as it progressively cooled from 300 K to 10 K (top curve) and then warmed back up to 300 K (bottom curve). The grain was exposed to a saturating field at 300 K prior to starting the measurements. The Verwey transition is marked by the split between the two curves at 112 K. The rise in moment at temperatures below ~100 K is probably a signature of superparamagnetic grains. The low temperature rise may also partly result from pyrrhotite's 34 K transition. The latter phase might also account for the fact that the cooling and warming curves remain split well below the Verwey transition (see inset).

standard Pyrex microscope slides using cyanoacrylate cement, and cut in Nanopure water with a 25 μm diameter diamond-impregnated continuous loop wire saw into a series of slices ~1 to 2 mm thick. Surfaces were then smoothed using wet 40-mesh diamond polishing paper. Each slice retained the relative orientation of the initial subsample, and was given a letter designation (e.g., 232a, 232b, 232c, etc.) in order of increasing distance from the original saw-cut surface. Because of visible metallic contamination and possible local heating from the original diamond-saw cut in Houston, we did not use the "a" sections in our magnetic imaging studies. Any shock remanent magnetization (SRM) from the sampling process, which tends to only affect low coercivity grains [21], is unlikely have remagnetized the crystals (coercivities up to ~60 mT) which unblocked during our heating experiments described later and could not have produced the multidirectional magnetization pattern that persists after heating to more than 200°C (see next Section).

4. Imaging of the Natural Remanent Magnetism in ALH84001

We imaged the perpendicular (east/west, in the meteorite orientation system) component of the magnetic field of the eight meteorite slices using the Ultrahigh Resolution Scanning SQUID Microscope (UHRSSM) (see Chapter 1). The version of this magnetometer used in this study has a sensitivity of better than 0.1 nT and is capable of making two-dimensional images of the magnetic field of materials at room temperature with a resolution of 500 μm. The UHRSSM is reported in [2, 6] and the general techniques of scanning superconducting quantum interference device (SQUID) microscopy are reviewed by [3, 4]. The application of SQUID imaging to geophysical samples was first demonstrated in [22]. The UHRSSM that produced our data employed a 500 μm diameter

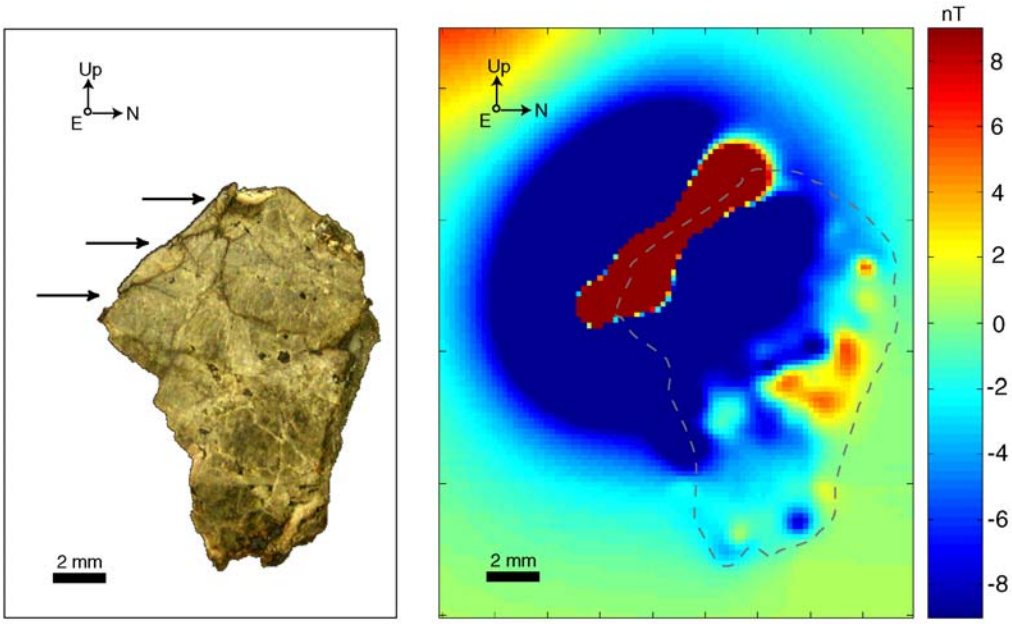

Fig. 2.2 UHRSSM image of ALH84001,228b. (**Left**) Photograph of oriented 1 mm thick slice that contains a small piece of the surface fusion crust (marked with arrows) oriented roughly normal to the image plane. This crust formed during entry through Earth's atmosphere. (**Right**) UHRSSM image of the same slice, displaying the east (out-of-the-page) component of the magnetic field at 250 μm above the slice. North is to the right and top is toward the top of the page, as demonstrated by the compass registered to the Johnson Space Center curatorial orientation system. An outline of the slice, corresponding to the edge of the slice in the photograph at left, is drawn around the sample. The color bar gives the field intensity in nT, with red and yellow (blue) corresponding to eastward (westward) magnetization. The fusion crust has been remagnetized by Earth's field in the east direction, with a peak intensity of ~1200 nT. A few millimeters toward the interior of the meteorite (i.e., to the lower right) the original heterogeneous pattern of magnetization is observable with amplitudes similar to those elsewhere inside the rock (Fig. 2.3). Scale bars, 2 mm.

superconducting NbTi pickup coil wound on a sapphire bobbin and held at 4.2 K. The coil is located in the vacuum space of the cryostat separated by a 25 μm thick sapphire window from the room-temperature ALH84001 samples, with a distance of ~250 μm between the coil and sample. Scans were made in a grid of 200 μm steps in a magnetically shielded room (DC field < 10 nT).

The fusion crust on the top-south surface of ALH84001,228b formed during its high-temperature passage through Earth's atmosphere and magnetic field, and is associated with an intense magnetic anomaly (Fig. 2.2). Moment magnetometry measurements of this and two additional samples with fusion crusts indicate that the meteorite initially came to rest in the ice with its east-southeast axis pointing up (assuming the fusion crust was above the Curie point until just before landing). Much weaker (~1% intensity) positive and negative magnetic features are present at distances of <5 mm in from the surface, implying that the heat pulse from atmospheric deceleration did not travel further than this into the meteorite. This shallow depth of heating is typical of most meteorites of this size [11]. These data suggest that the heterogeneous magnetization in the meteorite's interior (see also Fig. 2.3) predates arrival at Earth.

Using the same technique, we made multiple magnetic images of ALH84001,232e, which was extracted from the interior of the meteorite. The first image of the natural remanent magnetization (NRM) at room temperature (Fig. 2.3a) reveals a spatially heterogeneous pattern of magnetization like that observed in the interior portion of 228b. We also observed a similar, stable pattern in UHRSSM images of four other cm sized slices taken from the interior of the meteorite. In a second UHRSSM image of one of these slices taken 3 months later, the previously observed magnetization did not detectably change in pattern or intensity, giving strong evidence that the magnetization observed in Figs. 2.2 and 2.3 was stable during our experiments.

Several positive (eastward) and negative (westward) features are present (black arrows), some of which are dipolar in character. The strongest of these is centered on a carbonate bleb containing magnetite and pyrrhotite located 100 μm below the surface of the slice. In some regions, the dipolar features are centered on fractures (Figs. 2.3 and 2.4), while elsewhere fractures form the boundary

between pyroxene fragments that appear to be magnetized in different directions. The latter has been observed in previous studies of individual ALH84001 grains [18, 20].

At least three processes can have produced the spatial heterogeneity of the magnetization. The first is a brecciation event, in which fragments of the meteorite were rotated and translated with respect to one another without being heated. Such an event could explain the association between the magnetization pattern and rock fragments (e.g., the clast on the left side of 232e in Figs. 2.3 and 2.4). The second process is the deposition of several generations of magnetic minerals over a period during which the relative orientation of the local magnetic field changed. The latter could explain the dipolar and other magnetic features centered on fractures (e.g., those centered on the dashed cracks in Fig. 2.3). A third process is a series of shock events, which could have heterogeneously heated the rock on submillimeter scales, selectively remagnetizing isolated regions in the rock. Treiman [15] has identified five shock deformational events and a carbonate formation event. The earliest deformation, which he labeled D1, mobilized and rotated fragments of the rock, forming mm-thick cataclastic granular bands. Later events (D2b and D3) produced brittle fracture surfaces that transect the granular bands [15]. However, these events may have been too hot to produce a spatially heterogeneous magnetization [15, 23]. The fractures from D1 and D2b were then partly filled with the magnetized carbonate blebs (event Cγ) and also phyllosilicates [24]. We have correlated at least one dipolar feature centered over a crack with a carbonate bleb (Figs. 2.3 and 2.4). Some heterogeneity could also have been produced when the D3 event broke up and translated some of these carbonates [15, 23]. A low-temperature D4 event also may have brecciated the meteorite late in its history [15].

Regardless of which particular event(s) are responsible for randomizing the magnetization, it is fairly certain that ALH84001 was not brecciated during or after its ejection from Mars. Such a brecciation is highly unlikely to occur for orbital dynamical reasons [17, 25]. Furthermore, cosmic ray exposure studies demonstrate that ALH84001 was never shielded in a larger body in space [26]. The latter indicates that the meteorite lacked appreciable self-gravity and so could not also have been broken up and reassembled during the ejection process. Although there is evidence that terrestrial water has flowed through the meteorite [27, 28], the carbonates and their associated magnetic minerals originated on Mars [13]. It is unlikely that significant quantities of magnetic minerals were deposited in ALH84001 while on Earth, because the meteorite was mostly encased in ice in subzero temperatures and no secondary oxides have been identified other than those from Mars [15, 24]. Because the heterogeneous pattern of magnetization originated prior to ejection from Mars, it can be used to place a thermal constraint of the ejection and transfer of ALH84001 from the Martian surface to our laboratory.

5. Thermal Demagnetization

To determine the maximum temperature that ALH84001 experienced during its transfer to Earth, we progressively thermally demagnetized the meteorite. After producing the UHRSSM image of the NRM, slice 232e was first heated to 40°C for 10 min, cooled in an eastward 15 mT field, and then reimaged. It was then heated to 40°C for 10 min in a magnetically shielded furnace and cooled in a zero field (<10 nT) and reimaged. This cycle of heating and cooling was continued in 10 or 20°C steps up to 200°C. Oxidation of the iron-bearing phases was inhibited by first immersing the ALH84001 slices in mineral oil

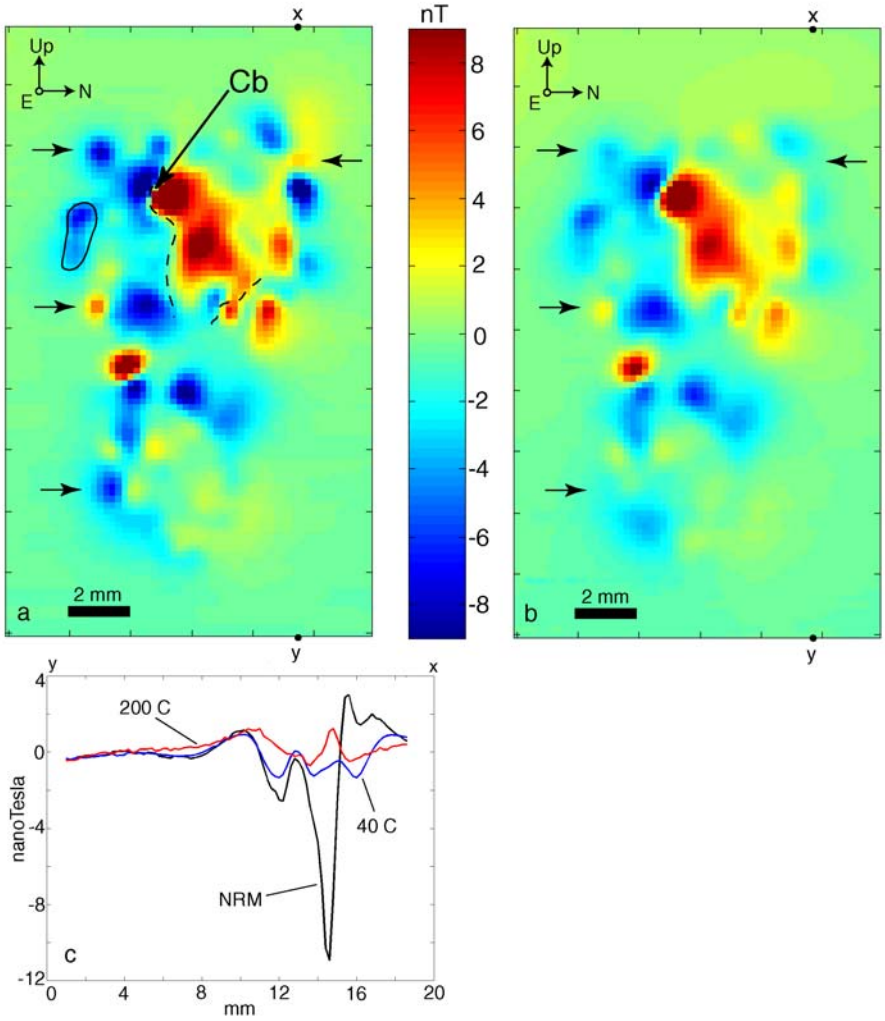

Fig. 2.3 UHRSSM images of ALH84001,232e. **a)** NRM of the oriented, 1 mm thick sample at room temperature before heating. Fracture surfaces on which two dipolar features sit are labeled with dashed lines. A fracture defining a distinctly magnetized grain is labeled with a solid line. A carbonate bleb containing magnetite and pyrrhotite was found 100 μm below the surface at the location labeled "Cb." **b)** Magnetization of the sample after being heated to 40°C for 10 min. The arrows in (a) and (b) indicate features that show significant decrease in intensity. Scale bars represent 2 mm and the color bar is in nT. **c)** Magnetic intensity variations along a line connecting points x and y, as observed in the unheated sample and after heating to 40°C and 200°C. This is a three-column running average centered on the line of pixels joining x and y.

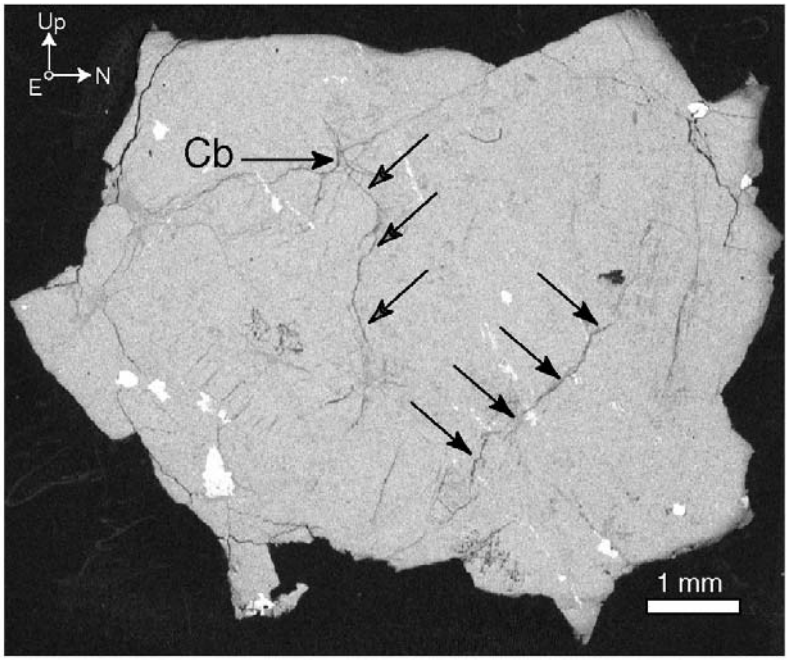

Fig. 2.4 Backscattered scanning electron microscopy image of top half of ALH84001,232e. Fractures (dark black lines), orthopyroxene (light gray), feldspathic glass (dark gray), and chromite (white) are visible. Both fractures labeled as dashes lines in Fig. 2.3a are visible and identified by a set of arrows. In one of them, a carbonate bleb containing magnetite and pyrrhotite was found 100 μm below the surface at the location labeled "Cb" (as in Fig. 2.3a). The carbonate bleb was observed after removal of a 100 μm thick layer from the original surface from which the magnetic map was obtained. The uniformly magnetized clast (defined by solid line in Fig. 2.3a) is visible at left. Scale bar, 1 mm.

containing an organic antioxidant (∝-tocopherol) and by removing trapped air under vacuum before each heating cycle. Following the heating to 40°C, the magnitude of many magnetic features decreased (including the dipolar feature centered on the carbonate) (Fig. 2.3b and c), completely erasing some that were present in the NRM scan (Fig. 2.3a). These features never regained the intensities

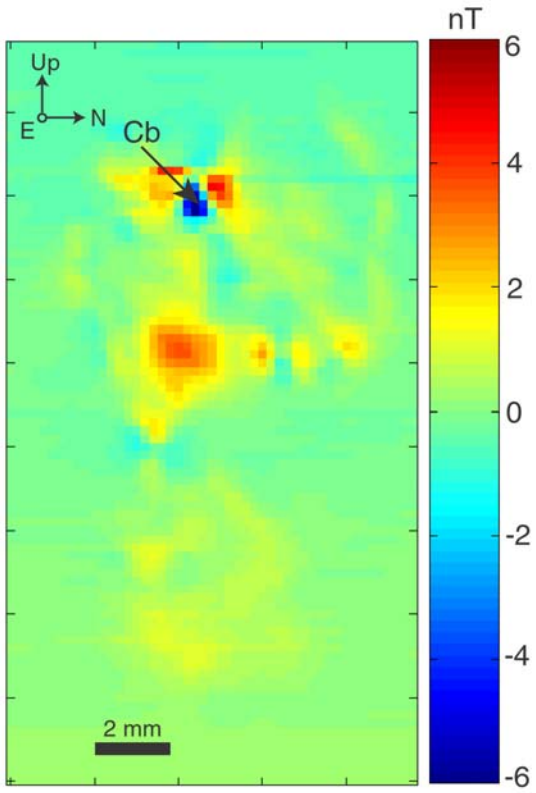

Fig. 2.5 Intensity difference between UHRSSM images of ALH84001,232e after heating to 200°C. Shown is the image taken after cooling in an eastward 15 mT minus image taken after cooling in a zero field. Prior to subtraction, images were spatially registered by maximizing their cross-correlation. The carbonate bleb identified in Figs. 2.3 and 2.4 is also labeled here ("Cb"). Scale bar, 2 mm. The background intensity gradient in the vertical direction is an artifact from instrument drift.

present in the NRM image. At each temperature step above 40°C, different randomly oriented features weakened or strengthened in magnetization. Our high-resolution transmission electron microscope (TEM) compositional maps (see Fig. 3.3 and Table 3.1) showed that in the carbonate rims, magnetite is only two to three times more abundant than pyrrhotite and both minerals have roughly similar crystal size distributions. On the other hand, a comparison of pyrrhotite's Pullaiah diagram (Fig. 2.6) with blocking temperature calculations for

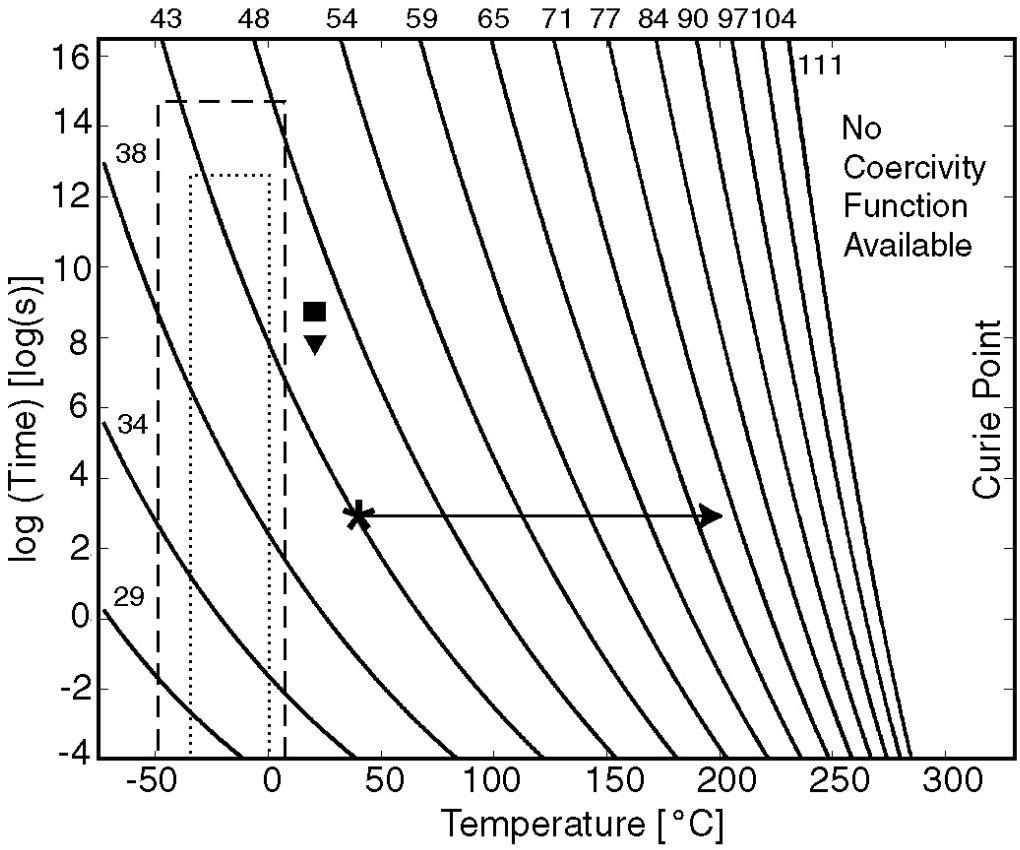

Fig. 2.6 Pullaiah diagram for monoclinic pyrrhotite (Fe_7S_8). This specifies the amount of time required to magnetize or demagnetize a SD crystal of a given size held at a given temperature. From left to right, curves are plotted for crystal diameters of 29, 34, 38, 43, 48, 54, 59, 65, 71, 77, 84, 90, 97, 104, and 112 nm. An arrow marks our 10 min heating experiments, which ranged from 40°C (asterix) to 200°C (arrow tip) in steps of 10°C or 20°C. This demonstrates that the 40°C heating unblocked all crystals smaller than 43 nm. Also marked are the likely conditions encountered while at Johnson Space Center (square: 14 years at 20°C) and Caltech (triangle: 2 years at 20°C). During its passage through space (15 Myr at temperatures between -50°C to 5°C) and time in Antarctica (11 Kyr from about -20°C to 0°C), ALH84001 experienced a range of conditions that lie somewhere inside the dashed box and dotted box, respectively. The diagram was calculated using the temperature dependence of microscopic coercivity and saturation magnetization as measured on crystals of diameter 200 to 1200 nm [29]. The coercivity function was measured in the temperature range of 20°C to 320°C, but did not give a good fit above 260°C [29]. The function was extrapolated down to -75°C and to crystal sizes of 29 nm for the purposes of this plot. An essentially identical Pullaiah diagram was independently calculated by Dunlop *et al.* [30].

magnetite (e.g., Fig. 3.5) shows that the range of pyrrhotite crystal sizes with blocking temperatures between room temperature and 40°C is an order of magnitude larger than that of magnetite. Assuming that the features which demagnetize are associated with carbonates, much of the magnetization that unblocked at 40°C should have been from pyrrhotite.

These minerals may have been susceptible to viscous remagnetization following ejection of the meteorite from Mars. Time-temperature calculations (see Appendix A1, Fig. 2.6 and [31]) suggest that pyrrhotites and magnetites with blocking temperatures below a few tens of °C and ~150°C, respectively, should be resistant to remagnetization and record an original Martian magnetization. Thus ALH84001 pyrrhotites (but possibly not magnetites) should be useful for placing low-temperature (<100°C) thermal constraints on the transfer of ALH84001 to Earth.

In the following discussion, we assume that the magnetic features that weakened during the thermal demagnetization are from pyrrhotite and are not a viscous remanent magnetism (VRM) (Appendix A1). We also make the conservative assumption that ALH84001 is not self-reversing and has an isotropic magnetic fabric (Appendix A2). As described in the Appendices, there are good reasons to believe that both of these assumptions are valid.

6. Thermal Constraint on the Transfer of ALH84001

The shortest thermal pulse that the meteorite could have experienced during the last 15 My is almost certainly that during the passage of a shock wave. The impactors capable of removing rocks from Mars, which are likely at least several km in diameter [25] and moving at a Keplerian velocity of ~10 km s^{-1}, would

produce a shock pulse of duration >~0.1 s [32] during collision with the martian surface. A shocked volume of rock equal to the pre-atmospheric size of ALH84001 would experience high post-shock temperatures lasting several hours [32] (see Chapter 4 for more details). Pyrrhotite's Pullaiah diagram (Appendix A1 and Fig. 2.6) demonstrates that crystals that magnetize after heating to 40°C for 10 min would also magnetize after heating to 125°C for 10^{-4} s or to 80°C for >~0.1 s. This means that any heating from a shock during ejection from Mars should probably have remagnetized pyrrhotites that demagnetized during our 10-min, 40°C laboratory heating step. Thus, our 40°C conglomerate test should be sensitive to both non-shock thermal pulses as well as to shock-heating.

If during its ejection, ALH84001 had been exposed to temperatures in excess of ~40°C and then cooled in a zero paleofield, no magnetic features would have changed in intensity during our 10 min heating experiment. If the meteorite had been heated to ~40°C and instead cooled in a local nonzero paleofield, features magnetized in the direction of that field would have weakened during our experiment, while the oppositely magnetized features strengthened. Because eastward and westward features (i) weakened by as much as 100% during demagnetization at temperature steps between 40°C and 200°C and (ii) ALH84001 magnetizes isotropically in the direction of an applied field, ALH84001 has most likely not been heated even 40°C since before it left Mars.

These results imply that ALH84001 was only lightly shocked during its ejection [8, 9] and therefore originates from near the planet's surface. Our data support recent suggestions [33, 34] that shock-implanted gases in ALH84001 did not enter the meteorite during ejection, but instead sample a martian atmosphere that is much older than 15 million years (see Chapter 4 for a more detailed investigation into the age of trapped atmospheric gases in ALH84001). Our results also indicate that major impact events are capable of moving rocks from

the surface of Mars to the surface of Earth without subjecting them to temperatures high enough to cause thermal sterilization of eukarya or bacteria. Dynamic simulations of martian impact events [9, 17, 25, 35] indicate that materials can be launched into a wide variety of orbits. Although most of the ~1 ton of martian rocks which land on Earth each year have spent several million years in space, one in 10^7 of the arriving rocks will have made the journey in less than a year [25]. Every million years, ~10 rocks larger than 100 g are transferred in just 2 to 3 years [25]. Bacterial spores, as well as microorganisms within rocks, can survive in deep space for more than 5 years [36]. These results indicate that it may not be necessary to protect Earth's present biosphere by quarantining rocks retrieved by a Mars sample return mission [37]. Conditions are appropriate to allow low-temperature rocks—and, if present, microorganisms—from Mars to be transported to Earth throughout most of geological time.

7. Other Thermal Constraints on ALH84001

This thermal constraint on the transfer of ALH84001 from Mars to Earth can be tested in variety of ways. A definitive future test for VRM should be successive thermal demagnetization of 30 μm thin sections (instead of 1 mm thick slices), imaging with a higher resolution UHRSSM sensor, and electron microscopic identification of the magnetization carriers in each UHRSSM image (e.g., Chapter 3). These changes would greatly simply inversion for the magnetization vector field in the sample (see Chapter 3). The retrieved magnetization solutions for each thermal demagnetization step could then be used for quantitative tests of randomness like that used in conglomerate tests with moment magnetometers [38]. SEM maps of the thin sections would also allow individual ferromagnetic minerals with low Curie points (e.g, pyrrhotite outside the carbonates, as well as chromite) to be distinguished from the

magnetite-bearing carbonates and specifically targeted for the conglomerate test.

Non-paleomagnetic methods like low-blocking temperature thermo-chronometers could provide independent constraints on the thermal history of ALH84001. In fact, our $^{40}Ar/^{39}Ar$ thermochronology (Chapter 4) demonstrates that the meteorite has been well below 350°C during the last 4 Ga. (U-Th)/He thermochronology on ALH84001 apatite, now in progress, could extend this constraint to even lower (<80°C) temperatures. Most significantly, the combined $^{40}Ar/^{39}Ar$ and petrographic data (Chapter 3 and 4) show that ALH84001 glass has not been shocked above its elastic limit of ~1 GPa since 4 Ga. This implies that the carbonates never have been shock-heated more than even a few degrees above ambient temperatures (~-90 to ~0°C) during ejection and transfer to Earth. In summary, these new data show that in fact ALH84001 was probably *well below* 40°C during its transfer from Mars to Earth. The exceedingly low temperatures of interplanetary space, rather than any high temperatures from ejection, may be a greater limit on the feasibility of panspermia.

Appendices

A1. Viscous Remanent Magnetism

As discussed at the beginning of Section 3, we detected no change in the magnetization pattern 232e over 3 months. This clearly demonstrates that the changes in magnetization observed during our laboratory heating steps are not a result of the progressive demagnetization of superparamagnetic grains that typically occurs after entrance into a shielded environment. In fact, viscosity

experiments with a moment magnetometer (Antretter *et al.*, manuscript in preparation) found that 1 minute following entrance into the shielded environment, no detectable changes occurred in the magnetization of a bulk grain of ALH84001.

A separate issue is whether or not the magnetization which unblocked after heating to 40°C originated on Mars or is instead a younger viscous remanent magnetism (VRM). To address this issue, we calculated a Pullaiah diagram [31] for monoclinic pyrrhotite using recently measured magnetization parameters [39]. The Pullaiah diagram gives the time required for an SD crystal to magnetize (in the presence of a field) or demagnetize (in zero field) at a given temperature (Fig. 2.6). Although the diagram is not always a reliable indicator of the behavior of natural crystal assemblages [40], it nevertheless suggests that any VRM acquired by ALH84001 while in Antarctica is unlikely to have affected pyrrhotite crystals with 10 min blocking temperatures of a few tens of °C and above. According to the diagram (Fig. 2.6), all crystals with 10 min blocking temperatures below ~50°C could have unblocked during ALH84001's 2-year stay in the Caltech shielded room before the start of our experiments. This would seem to include any VRM acquired while in Antarctica and SRM from sample preparation, as well as the magnetization that unblocked during our 40°C heating step (Figs. 2.3 and 2.6). The diagram also suggests that residence at the Johnson Space Center may have remagnetized crystals with 10 min blocking temperatures below ~65°C. Passage through the low-field (several nT) environment between Mars and Earth is unlikely to have left a VRM, but may have demagnetized pyrrhotite crystals with 10 min blocking temperatures below ~80°C (Fig. 2.6).

On the other hand, the diagram (Fig. 2.6) is untested and required extrapolation of a coercivity function that was measured on temperatures only down to 20°C and on crystals (sized 100 nm to 30 mm) larger than those in the diagram [29].

The Pullaiah diagram for magnetite has disagreed by several orders of magnitude with other theoretical treatments as well as some experiments [40]. Most importantly, ALH84001 thermally demagnetizes steadily and *in a spatially heterogeneous manner* from 40°C to 200°C. Because grains of a given blocking temperature should acquire a VRM *in the same direction*, this suggests that most of the magnetization that unblocked during the 40°C heating step was probably not a VRM but instead a remanence acquired while on Mars. Nevertheless, if the diagram (Fig. 2.6) is taken as correct, then in the most stringent scenario (that ALH84001 spent several My at 5°C while in space, such that all grains with 10-min blocking temperatures below 80°C were remagnetized) the thermal constraint on ALH84001 since before ejection would become 80°C.

A2. Magnetic Fabric

With rare exceptions, most rocks magnetize uniformly in the direction of the local magnetic field when they cool below their Curie temperatures or when their magnetic minerals crystallize out of a low-temperature solution. The few known examples of rocks that acquire a TRM that varies in direction within the sample are those with strong magnetic anisotropy and/or self-reversing tendencies [40]. Neither of these properties should be present in ALH84001. Although individual crystals can exhibit magnetocrystalline or shape anisotropy, this could not effect the gross magnetization of cumulates like ALH84001 in which the crystals are randomly oriented. Highly foliated rocks can acquire magnetic anisotropy due to alignment of the crystals, although this has not been noted for the heavily shocked Apollo samples [41]. Four mechanisms of self-reversed magnetization (magnetization in a direction opposite that of other nearby grains and the background field) have been reported [40]. Three of these are only known to occur in the presence of high-Ti iron oxides [40], none of which have

been identified in ALH84001 [19]. The fourth has been observed in large MD synthetic magnetic grains with exsolved magnetic minerals, but has never been conclusively identified in natural samples [40, 42, 43]. It is unlikely to occur in ALH84001, which contains PSD and smaller crystals and lacks detectable exsolution features in any minerals [44]. We conclude that ALH84001 should have been capable of isotropically acquiring a thermoremanent magnetization (TRM) during our heating experiment and throughout its 4.5 billion-year history.

This conclusion is supported by two experiments. In the first, we subjected the large pyroxene grain studied by Kirschvink *et al.* [18] to three 100 mT magnetic pulses at room temperature to give the grain an IRM, which we measured after each pulse. After the first and second pulses, the grain was rotated 90° along the north and east directions, respectively, while keeping the field direction constant. In all three cases the magnetic phases in the grain remagnetized with the same intensity to within 1° of the field direction.

In our second experiment, we compared the magnetization image obtained after heating to 200°C and cooling in the eastward 15 mT field with that obtained after heating to the same temperature and cooling in the zero field (Fig. 2.5). Almost the entire slice remagnetized in the eastward direction. The region with westwardly oriented fields (at the top center of Fig. 2.5) is centered on a carbonate bleb (Fig. 2.4). Note that because this is a map of fields (not magnetization), these reversed fields do not require that the rock has magnetic anisotropy or is self-reversing. If the field in which the meteorite acquired its NRM was less than 15 mT, then westwardly oriented fields could increase after laboratory heating at low temperatures since the newly acquired magnetization, although pointing eastward, is also higher in intensity than the magnetization it replaced. Some of this apparent anisotropy is also likely to be an artifact resulting from pixelation noise, imperfect registration of the

subtracted images, and differences in heating and cooling time between the zero field and 15 mT field steps. Because the westwardly magnetizing region is much more strongly magnetized than the rest of the slice, the differences in heating and cooling time will affect this feature more strongly. In summary, our theoretical expectations and experiments both strongly suggest that the meteorite has an isotropic magnetic petrofabric.

Chapter 3

RECORDS OF AN ANCIENT MARTIAN MAGNETIC FIELD IN ALH84001[3]

Although Mars does not presently appear to have a global dynamo magnetic field, strong crustal fields have recently been detected by the Mars Global Surveyor above surfaces formed ~3 or more billion years ago (Ga). We present magnetic and textural studies of martian meteorite ALH84001 demonstrating that 4 billion year old carbonates containing magnetite and pyrrhotite carry a stable natural remanent magnetization. Because our $^{40}Ar/^{39}Ar$ thermochronology demonstrates that most ALH84001 carbonates have probably been well below the Curie point of magnetite since near the time of their formation, their magnetization originated at 3.9 to 4.1 Ga on Mars. This magnetization is at least 500 million years (Myr) older than that known in any other planetary rock, and its strong intensity suggests that Mars had generated a geodynamo and global magnetic field within 450 to 650 Myr of its formation. The intensity of this field was roughly within an order of magnitude of that at the surface of the present-day Earth, sufficient for magnetotaxis by the bacteria whose magnetofossils have been reported in ALH84001 and possibly for the production of the strong crustal anomalies. Chromite in ALH84001 may retain even older records of martian magnetic fields, possibly extending back to near the time of planetary formation.

---

[3] Adapted from: Weiss, B. P., H. Vali, F. J. Baudenbacher, J. L. Kirschvink, S. T. Stewart, D. L. Shuster (2002) Records of an ancient Martian magnetic field in ALH84001, *Earth Planet. Sci. Lett.*, **201**, 449-463.

1. Introduction

The age of the crustal magnetization on Mars has been interpreted to be either older [45] or substantially younger [46] than several large, ~3.0 to 4.2 Ga impact basins. At least 11 martian meteorites have remanent magnetizations [20, 47-52] that originated sometime after the rocks formed at 1300-180 Ma. Another martian meteorite, ALH84001, is an orthopyroxene cumulate which crystallized at 4.5 Ga [12] and contains ~1% zoned carbonate. These carbonates contain magnetite and iron sulfide [19] and have Rb/Sr and Pb/Pb ages of 3.90 ± 0.04 Ga and 4.04 ± 0.1 Ga, respectively [14] (although the Rb/Sr data have recently been questioned [53]). As described in Chapter 1, ALH84001 also possesses a stable magnetization that predates its ejection from Mars 15 million years ago (Ma) [5, 18, 20]. Because it is the oldest known martian rock, ALH84001 may contain unique records of the earliest period of martian magnetism and evolution [54].

Kirschvink *et al.* [18] argued that iron sulfide within the orthopyroxene of ALH84001 carries a stable magnetization, but were unable to demonstrate that the meteorite's carbonates are magnetized. Based on a paleomagnetic conglomerate test on two adjacent ALH84001 orthopyroxenite grains, they suggested that the meteorite has been cooler than 110°C since before the formation of the fracture surface separating the grains. They assumed this fracture was part of the internal crushed zone created during the "D1" shock event [15]. However, subsequent studies (see Section 5) have identified flow textures and vesicles in feldspathic glass that intrudes and disrupts carbonates, suggesting that one or more high-temperature shock events (with peak pressures of >45 GPa and temperatures >1400°C) affected at least part of the meteorite after the D1 event [15, 23, 55]. Because no carbonates were identified on the fracture surface separating Kirschvink *et al.*'s two grains, this

fracture need not have formed during D1 but instead could date to any time between 4.0 Ga and 15 Ma. Thus, their thermal constraint may not apply to before the time of carbonate formation, but instead extend back to a more recent but unknown time. More detailed magnetic studies by Weiss *et al.* [5] (described in Chapter 1) have shown that the transfer of ALH84001 from Mars to their laboratory, including the impact at 15 Ma that ejected it from the martian surface and its passage through the Earth's atmosphere, did not heat the interior of the meteorite above a few tens of ◦C for even short periods of time (<10 min). It is unknown how much further back in time beyond 15 Ma that thermal constraint applies.

2. Samples and Methods

We analyzed two unoriented and two oriented subsamples of ALH84001 for this study. ALH84001,232e (Figs. 3.1, 3.2, 3.3) is a 1 mm thick slice from the interior of the meteorite previously studied by Weiss *et al.* [5]. Slice 232e was cut from subsample ALH84001,232 with a diamond-impregnated wire saw and mounted on a glass slide with cyanoacrylic cement [5]. An unoriented subsample of ALH84001,236 was used for high-resolution transmission electron microscopy (TEM) imaging (Fig. 3.4). TEM data on 594 individual ALH84001 magnetite crystals used for our blocking temperature calculations (Fig. 3.5) were measured by Thomas-Keprta *et al.* after extraction from another unoriented subsample [19].

Our anhysteretic remanent acquisition studies (Fig. 3.6) were conducted on a second unoriented pyroxenite grain from ALH84001,236 weighing ~20 mg and containing zoned carbonate. Finally, subsample 227b (Figs. 3.7, 3.8, 3.9) is an oriented 30 μm thin section taken from near the meteorite's fusion crust. The

thin section was set with cyanoacrylic cement at room temperature so that its natural remanent magnetization (NRM) was preserved. ALH84001,232e and 227b were also both analyzed with backscatter scanning electron microscopy (SEM) (Figs. 3.1, 3.2 and 3.8).

Field emission gun transmission electron microscopy (FEG-TEM) data were taken from an ultrathin section prepared from a zoned carbonate in 232e (identified in [5] and in Fig. 2.3), taken from just below the tip of the bottommost arrow in Fig. 3.1a using a micro sampling device on a Hitachi FB-2000A focus ion beam system (Fig. 3.2). This system allows non-destructive preparation of an ultrathin section in situ with a precision of 1 μm without exposing the sample to water, epoxy resin, or other contaminants. The bright field (Fig. 3.3a,e), compositional (Fig. 3.3b-d), and selected area electron diffraction (Fig. 3.3e, inset) data were acquired on this section with a Hitachi HF 2200 cold field emission analytical TEM, using an acceleration voltage of 200 kV and a camera length of 80 cm. The patterns of single crystal and polycrystalline magnesite present in the section were used as an internal standard. The lattice plane spacings, d, were calculated using the formula $d = \lambda L/r$, where λ is the wavelength of the electron beam at 200 kV, L is the camera length and r is the distance of a given pattern to the center of the primary beam (see Table 3.1). As the center of the primary beam cannot be accurately determined, the value of r is measured from the distance between two radially symmetrical patterns divided by 2. The diffraction pattern was taken from a selected area on a low magnification image (10,000 ×).

To conduct the anhysteretic remanent magnetism (ARM) acquisition test, we demagnetized the samples using a sinusoidally oscillating alternating field (AF) whose amplitude decayed from 100 mT to zero. We then gave the sample an ARM by subjecting it to a 0.2 mT DC bias field superimposed on the same AF. The intensity of magnetization of the sample was measured, and then the grain

was given a new ARM with a larger DC bias field and its magnetization remeasured (Fig. 3.5). This process was repeated until reaching a bias field of 2 mT. Control ARM acquisition tests were measured using the same protocol on MV-1 magnetotactic bacteria and chiton teeth. All of the above magnetic measurements were made with a 2G® Superconducting Rock Magnetometer in a class 1000 magnetically shielded (field <100 nT) clean laboratory at Caltech.

Images of sample magnetic fields were obtained with the ultra high-resolution scanning SQUID microscope (UHRSSM) [2, 6], a DC-SQUID magnetometer with a DC-field sensitivity of ~75 pT that maps the perpendicular component of the magnetic field of samples with better than 250 μm spatial resolution. SQUID microscopes with somewhat lower sensitivity and spatial resolution have been used in a variety of previous paleomagnetic studies [5, 22, 56-58]. The UHRSSM measurements were made in a magnetically shielded environment at Vanderbilt University (field <10 nT).

3. The Magnetized Minerals in ALH84001

To determine the mineralogy of the magnetic phases in ALH84001, we conducted SEM (Figs. 3.1a and 3.2) and FEG-TEM analyses (Figs. 3.2 and 3.3 and Table 3.1) of the Fe-rich rim of a carbonate in ALH84001,232e. These data demonstrate the presence of magnetite (Fe_3O_4) and pyrrhotite ($Fe_{1-x}S$ for $x < 0.13$) in the carbonate rims. FEG-TEM compositional maps of Fe, S, Mg (Fig. 3.3a-d), O, Mn, K, Al and Ca (not shown) taken from the same location resolve individual crystals of pyrrhotite and magnetite in the single domain (SD) to superparamagnetic (SP) size range. Our SEM and FEG-TEM imaging (Figs. 3.1a and 3.2) show that a typical zoned carbonate is composed of ~1 wt% pyrrhotite

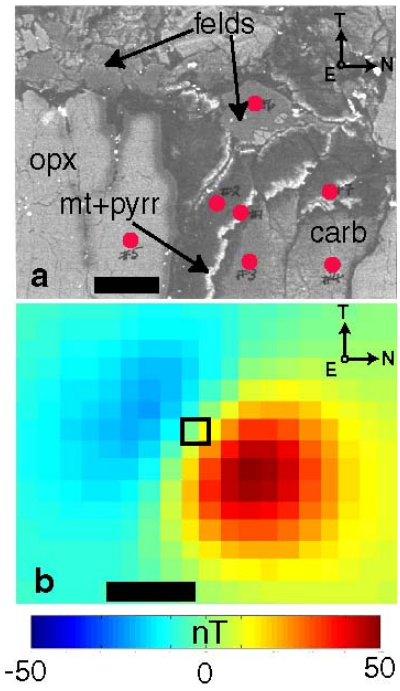

Fig. 3.1 Compositional and magnetic maps of part of ALH84001,232e. These images are centered on the carbonate found ~100 μm below the surface by Weiss *et al.* [5] (see Figs. 2.3 and 2.4). **a)** Backscattered SEM image showing orthopyroxene, zoned carbonate (with dark Mg-carbonate rim bounded by two bright bands of magnetite and pyrrhotite), feldspathic glass, and fractures (dark black lines). The compositions of these phases were confirmed by X-ray spot analyses taken at the locations marked by red circles. A cross section of the carbonate was later extracted for FEG-TEM analyses (Fig. 3.3) from the boundary between the Mg-carbonate and inner band of magnetite and pyrrhotite, just below the tip of the bottom arrow (Fig. 3.2). **b)** Ultrahigh resolution scanning SQUID Microscope (UHRSSM) image centered on same location as a, showing the intensity of the eastward (out-of-the-page) component of the magnetic field as observed ~200 μm above the sample. The sample had been heated to 360°C in a zero field (<10 nT) prior to UHRSSM imaging. The SEM image in (a) was taken from roughly the location marked by the black box at the center. North is to the right and Top is toward the top of the page, as demonstrated by the compass registered to the Johnson Space Center curatorial orientation system. Red (blue) regions correspond to eastwardly (westwardly) oriented fields. Scale bars are 20 μm (a) and 500 μm (b), and the color bar is in nT.

and magnetite in a mass ratio of ~0.3 to 0.5. This mineralogy is also indicated by our high-resolution TEM data from another carbonate in ALH84001,236 (Fig. 3.4). Our rock magnetic analyses on three ~15 mg ALH84001 pyroxenite grains containing carbonates [5, 18] again demonstrate that the meteorite contains magnetic crystals ranging from SP to PSD in size. Thomas-Keprta *et al.* [19]

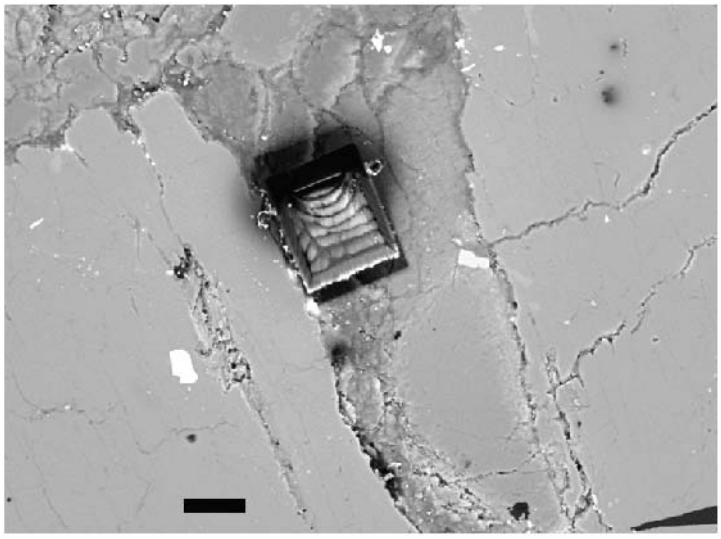

Fig. 3.2 Ultrathin section preparation from ALH84001,232e. Shown is a backscattered SEM image of carbonate from ALH84001,232e (at location just below bottommost arrow in Fig. 3.1a) after the ultrathin section was prepared for FEG-TEM analysis (Fig. 3.3). A micro sampling device on a Hitachi FB-2000A focus ion beam (FIB) system progressively milled into the sample, producing an ultrathin section 20 μm wide by 20 μm long by 80 nm thick. The ultrathin section was initially prepared by cutting a wedge of thickness 5 μm by combined step and trench milling. The wedge was transferred and mounted on a compatible FIB/TEM holder using a mechanical probe. To reach the desired thickness and location of the ultrathin section, the wedge was then gradually ion-milled by transferring the specimen back and forth between the FIB and the TEM. A scanning mode in both FIB and TEM was used to monitor this procedure. This system allows non-destructive preparation of an ultrathin section *in situ* with a precision of 1 μm without exposing the sample to water, epoxy resin or other contaminants. The scale bar is 20 μm.

found that 594 individual magnetite crystals extracted from the carbonate are nearly stoichiometric (Ti, Al, and Cr < 0.1%) and in the SD (~70% of grains) to SP (~30% of grains) size range. Low temperature cycling [5] indicates that ALH84001 magnetites have a composition $Fe_{3-x}Ti_xO_4$ with $x \approx 0.01$. Magnetite of this composition has a Curie point of close to 580◦C [40]. Thermal demagnetization of ALH84001,232e [5] demonstrates that the meteorite has blocking temperatures from less than -263◦C to well in excess of 200◦C. Our data presented below (Fig. 3.1b) further extend this range by demonstrating that the meteorite remains strongly magnetized after zero-field heating to >360◦C. A comparison of the size and shape distribution measured by Thomas-Keprta *et al.*

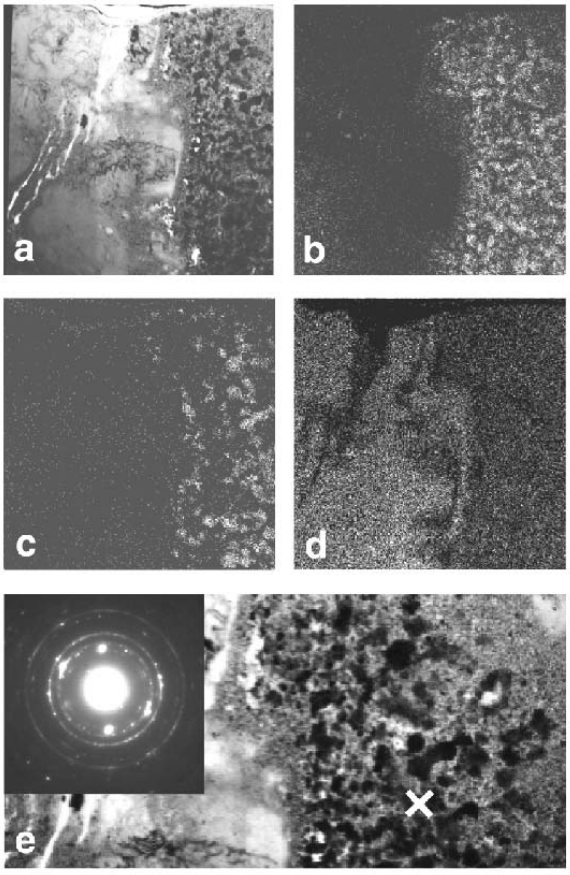

Fig. 3.3 Field emission gun transmission electron microscopy (FEG-TEM) data on ALH84001,232e carbonate. Shown are the fine-grained particles present within the rim of the carbonate from ALH84001,232e identified by Weiss *et al.* [5] (see Figs. 2.3 and 2.4). As depicted in Fig. 3.2, a vertical slice of thickness ~80 nm was prepared perpendicular to the image plane in Fig. 3.1. **a)** High-resolution bright field image showing individual magnetite and pyrrhotite crystals embedded in Mg-Ca-Fe-carbonate (right) adjacent to Mg-carbonate rim (left). **b-d)** High-resolution (1 nm) X-ray compositional maps of same region as a showing abundance of Fe (b), S (c), and Mg (d). A comparison of (b) and (c) with our O maps taken from the same location (not shown) shows that many individual crystals simultaneously contain either Fe and S or Fe and O, demonstrating the presence of iron sulfides and iron oxides. **e)** Higher magnification bright field image taken from top of (a), with superimposed selected area electron diffraction pattern measured at the location marked by ×. The lattice plane spacings corresponding to the pattern are diagnostic of pyrrhotite (4.73, 2.61, and 2.06 Å), magnetite (4.84 and 2.53 Å), and Mg-carbonate (2.75 and 2.11 Å). For a complete list of observed lattice plane spacings, intensities and their corresponding Miller indices, see Table 3.1. Each frame in (a-d) has a width of 7 μm, and frame (e) has a width of 5 μm.

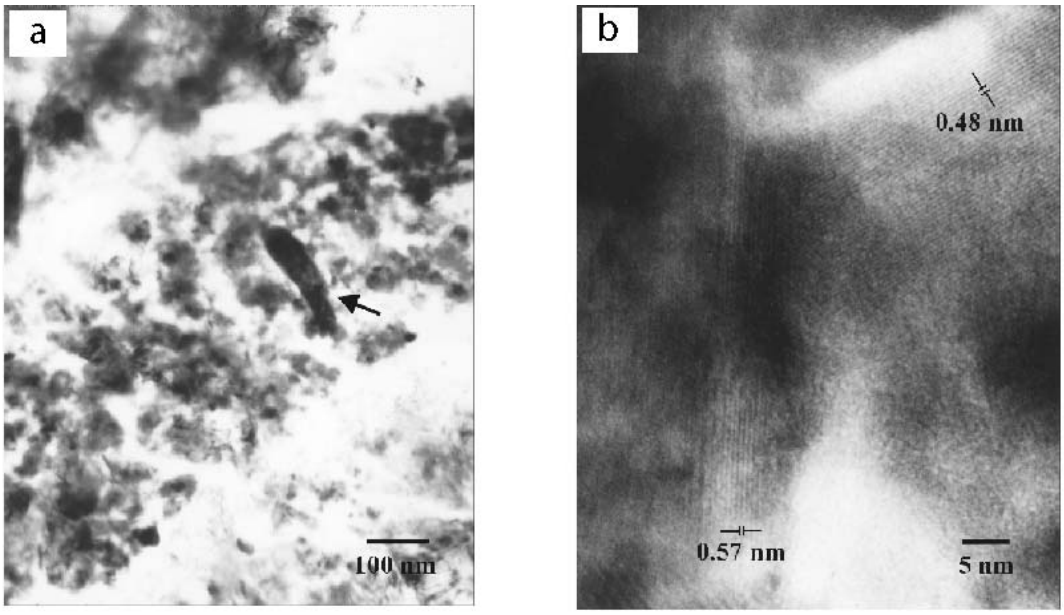

Fig. 3.4 High-resolution TEM images of the rim of an ALH84001 carbonate. **a)** Low magnification image showing iron sulfide (arrow) and iron oxide in Fe-rich rim of the zoned carbonate. **b)** High-resolution image of the edge of the sulfide and an adjacent oxide showing the lattice fringes of 0.48 nm and 0.57 nm, diagnostic of pyrrhotite ($Fe_{1-x}S$ for $x < 0.13$) and magnetite (Fe_3O_4), respectively. Greigite, whose lattice also has a 0.48 nm spacing, is unstable under the electron beam and so cannot explain these data (e.g., [59]).

[19] with our Néel theory calculations of the temperature dependence of the SP-SD boundary confirms that the ALH84001 magnetites have blocking temperatures up to 580°C (Fig. 3.5). These observations demonstrate that, despite suggestions to the contrary [51], stoichiometric magnetite should dominate the remanent magnetism of carbonates in ALH84001 (with pyrrhotite only significantly contributing to the low blocking temperature fraction).

The tight packing of the magnetite and pyrrhotite in the carbonates (Fig. 3.3) suggests that these crystals should be magnetostatically interacting. We examined this possibility using an ARM acquisition test on a subsample of ALH84001,236 (see Section 2). The linearity and shallow slope of the meteorite's ARM

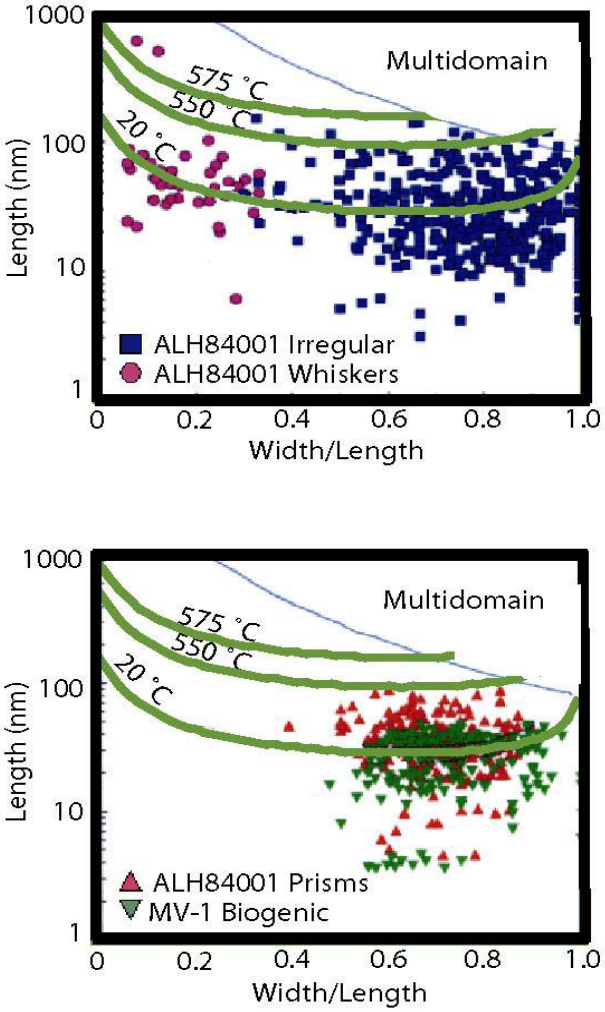

Fig. 3.5 Crystal size, shape and blocking temperature distribution of magnetite in ALH84001 carbonate. Blocking temperatures have been calculated as a function of size and shape and are compared to the natural size distribution of inorganic (**Top**) and fossil-like (**Bottom**) magnetite. Each green curve represents the SD-SP boundary for various temperatures as a function of crystal length and crystal length-to-width ratio. We assume a parallelepiped grain shape (as has been observed for ALH84001 magnetite [19]) and an unblocking time of 100 s. We calculated these curves following the methods of Butler and Banerjee [60] as modified by Diaz Ricci and Kirschvink [61]. The blue curve in each diagram represents the single domain-multidomain boundary. The curves have been overlaid onto the actual distribution of magnetite in ALH84001 carbonate, as measured by Thomas-Keprta *et al.* [19]. The diagrams demonstrate that ALH84001 carbonates contain magnetite with blocking temperatures up to its Curie point of 580◦C.

SAED *d*-spacing (Å)	Mineral name	Reference *d*-spacing (Å)	Miller indices (*hkl*)
4.84	magnetite	4.852	(111)
4.73	pyrrhotite	4.7	(113)
2.75	magnesite	2.742	(104)
2.61	pyrrhotite	2.633	(224) (404)
2.53	magnetite	2.532	(311)
2.42	magnetite	2.424	(222)
2.11	magnesite	2.102	(113)
2.06	pyrrhotite	2.054	(228)
1.96	magnesite	1.939	(022)
1.71	magnesite	1.7	(116) (018)
1.61	magnetite	1.616	(511)
1.36	magnesite	1.354	(119)
1.26	magnetite	1.266	(622)

1.06	magnesite	1.051	(226)
0.88	magnetite	0.88	(931)
0.80	magnetite	0.808	(1022)

Table 2.1 Mineralogy of ALH84001 carbonate rims. Shown are minerals identified by selected area electron diffraction analysis (SAED) on an ultrathin section from the Fe-rich area in ALH84001,232e (Fig. 3.3). Shown is a list of the *d*-spacings (first column) and their corresponding mineral name (second column) for the diffraction patterns observed in the SAED image (Fig. 3.4e inset). The X-ray reference *d*-spacings obtained from the Powder Diffraction File Database and their associated Miller indices (*hkl*) are listed in the third and fourth columns, respectively.

acquisition curve (Fig. 3.6) gives strong evidence of magnetostatic interactions. Additional evidence for these interactions comes from the fact that both this grain and ALH84001,190 (the latter studied by Kirschvink *et al.* [18]) have isothermal remanent magnetism (IRM) acquisition and AF demagnetization of IRM curves that intersect at about 35% of the saturation IRM. The presence of these interactions indicates that it might be difficult to use standard techniques [62, 63] to precisely measure the paleointensity of the field that magnetized ALH84001.

4. SQUID Microscopy

We have used the UHRSSM to map the vertical component of the remanent magnetic fields of ALH84001,227b,1 (Figs. 3.7 and 3.8) and a carbonate [5] from ALH84001,232e (Fig. 3.1; see also Figs. 2.3 and 2.4). In order to examine the thermal stability of the magnetization in the meteorite, 232e was progressively

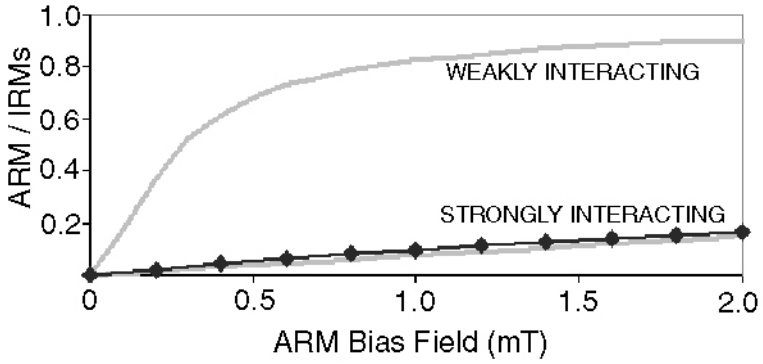

Fig. 3.6 Anhysteretic remanent magnetism (ARM) acquisition experiments on ALH84001. The subsample was a ~20 mg pyroxenite grain with zoned carbonate taken from ALH84001,236. Shown is the anhysteretic magnetic moment (normalized to the isothermal saturation magnetic moment) of three samples for a given DC bias field (see Section 2): ALH84001,236 (heavy black line), non-interacting MV-1 bacterial magnetosomes (top gray line), and highly interacting chiton tooth magnetite (bottom gray line).

thermally demagnetized at temperatures up to 360◦C in a zero field (<10 nT) prior to final imaging with the UHRSSM (Fig. 3.1b). A comparison of the UHRSSM data with the electron microscopy and X-ray spot analyses shows that nearly all of the magnetic fields above the interior of these samples are directly associated with zoned carbonate, identified in both 227b (Fig. 3.8c-f,h,k-m) and 232e (Figs. 3.1 and 3.3), and a few irregular unzoned carbonate patches, as identified in 227b (Fig. 3.8c,d). The latter carbonates are more calcic than the zoned carbonates and do not show a distinct, Fe-rich and Mg-rich rim (similar unzoned carbonates were recently identified by Eiler *et al.* [64] as the likely products of shock-melting of zoned carbonate). Several chromite grains also exhibit a weak magnetization (Fig. 3.8a,b,e,f,j). The 0.1 mm thick fusion crust on the exterior of the meteorite (Fig. 3.8b,d,g) was produced during passage through Earth's atmosphere during which it was strongly magnetized by Earth's field (Fig. 3.8a,c). As has been previously observed [5], this remagnetized zone extends no further than ~1 mm into the interior of the meteorite. A

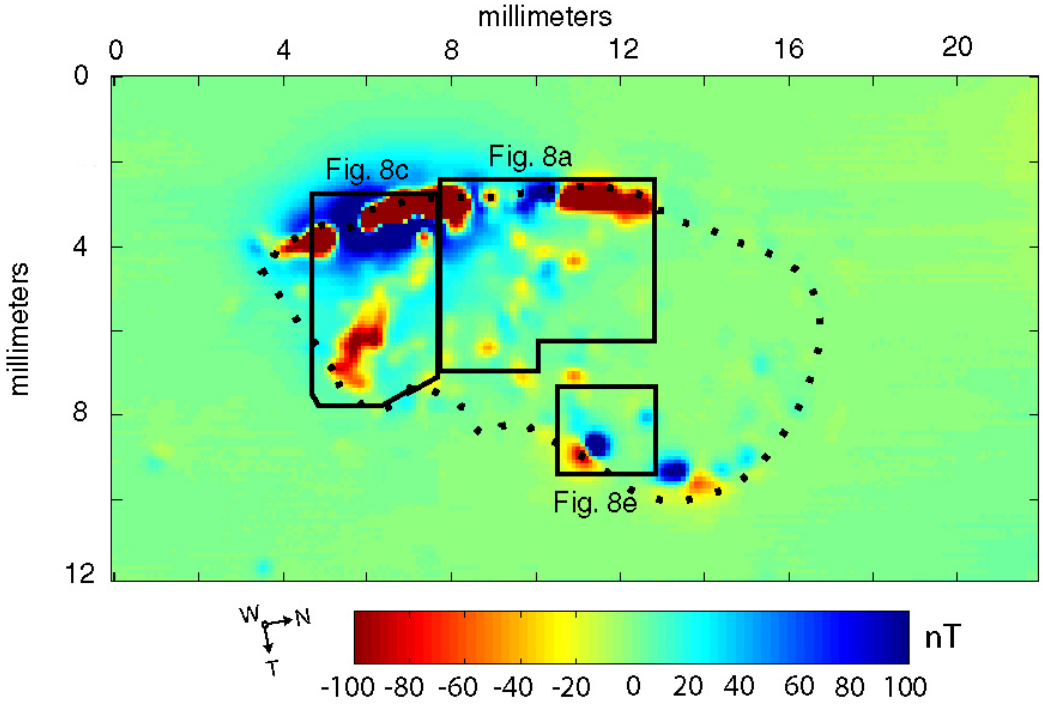

Fig. 3.7 The complete UHRSSM scan of ALH84001,227b,1. Shown is the westward (out-of-the-page) component of the magnetic field ~130 μm above the sample. The boxed regions correspond to the various parts of 227b imaged in Fig. 3.8. The border of the thin section has been outlined with a dotted line on the UHRSSM scan. The compass is registered to the Johnson Space Center curatorial orientation system.

comparison of UHRSSM images of the carbonate in 232e taken before heating [5] (Fig. 2.3) and after thermal demagnetization at temperatures of 360°C (Fig. 3.1b) confirms our expectation that the carbonate has magnetic blocking temperatures from room temperature to well beyond 360°C. Other than the magnetite, pyrrhotite, fusion crust, and chromite, we did not identify any other ferromagnetic grains in the 227b thin section; no other magnetic features in the UHRSSM map can be associated with other minerals, and no other ferromagnetic minerals have ever been found in the meteorite.

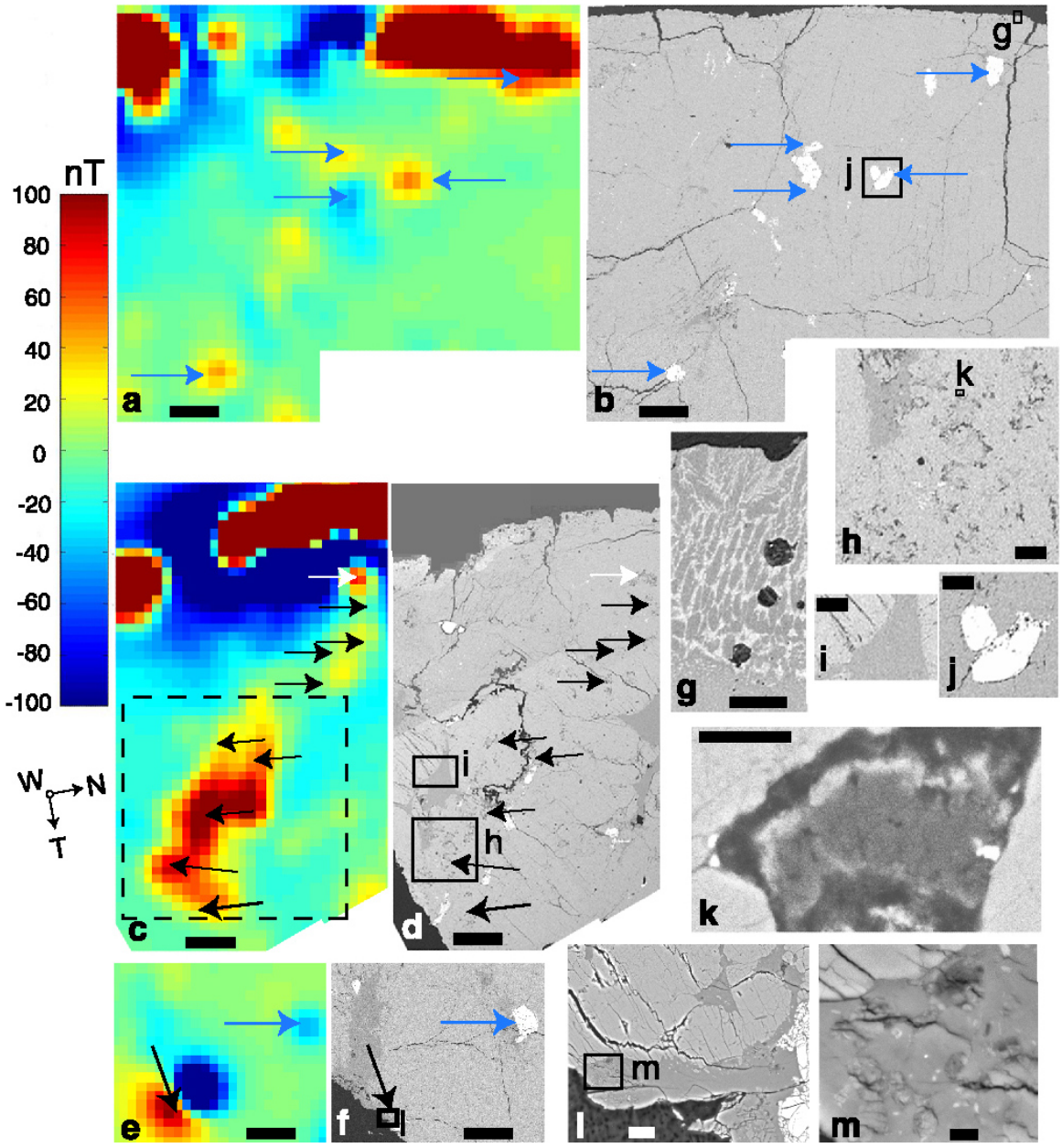

Fig. 3.8 Magnetic and compositional maps of selected portions of ALH84001,227b,1. For the complete magnetic map, see Fig. 3.7. a**)** UHRSSM image showing westward (out-of-the-page) component of the magnetic field ~130 μm above the sample. The compass is registered to the Johnson Space Center

curatorial orientation system. **b)** Backscattered SEM image of same field as (a) showing orthopyroxene (light gray), feldspathic glass (dark gray), chromite (white grains, including those marked by blue arrows), and fusion crust discontinuously lining the top of the sample. The ~0.1 mm thick fusion crust was strongly magnetized during the meteorite's passage through the Earth's atmosphere. **c,d)** UHRSSM and SEM images of a different portion of the same thin section with zoned carbonate containing magnetite and pyrrhotite (black arrows) and unzoned carbonate (white arrow). Strongly magnetized fusion crust lines the top of the sample, with a notch in the middle. A least squares magnetization inversion for the UHRSSM data enclosed by dashed box in (c) is presented in Fig. 3.9. **e,f)** UHRSSM and SEM images of a different portion of the same thin section with magnetized chromite (blue arrow) and zoned carbonate (black arrow) containing magnetite and pyrrhotite. **g-m)** Higher magnification SEM images of selected portions of (b), (d), and (f): fusion crust (g); two lightly fractured, subhedral magnetized chromites (j); unfractured feldspathic glass surrounded by fractured orthopyroxene (i) that is adjacent to a patch of magnetized carbonate in a granular band of orthopyroxene (h,k); heavily fractured zoned carbonate that has been disaggregated and transported by feldspathic glass (l,m). Carbonate is dispersed throughout most of the glass visible in l. Magnetized chromites are labeled with blue arrows in (a),(b),(e),(f). Scale bars are 500 μm (a-f), 100 μm (h-j), 20 μm (g,l), and 3 μm (k,m).

Most of the magnetization associated with the carbonates is stable and remanent. Langevin theory [40] demonstrates that a typical ALH84001 carbonate (with a radius of ~50 μm and containing ~10^8 SP and SD grains of magnetite and pyrrhotite) immersed in a 10 nT laboratory field will produce an induced magnetic field of <0.1 nT at the height of the UHRSSM pickup coil. Because the UHRSSM measures fields of ~100 nT above single carbonates like that in Figs. 3.1b and 3.8e, their magnetization cannot be induced but must be a remanence. Furthermore, magnetite's Pullaiah diagram [40] suggests that ALH84001 magnetites with 10 min blocking temperatures ~>150°C would not acquire viscous remanence during residence on the martian surface (assuming <-50°C for 4 Gyr), transfer through space to Earth (assuming <0°C for 15 Myr), and residence in Antarctica (assuming <0°C for 11 kyr) and America (<20°C for 17 yr).

To confirm that the carbonates, chromite, and fusion crust are actually the source of the magnetic field observed with the UHRSSM, we performed inversions to obtain the magnetization distribution that best reproduces (in a least squares sense) the fields above 227b. Although there is in general no unique magnetization distribution that can be associated with measurements of a given magnetic field pattern outside a magnetized region, such an inversion can be

made solvable by assuming that the sample's magnetization is in the form of a grid of *N* evenly spaced dipoles confined to a plane within the sample. This two-dimensional "equivalent source" method provides a good approximation for retrieving the magnetization of the 30 μm thin section 227b, whose magnetic field was measured at a height ~4 times its thickness. The method, commonly employed to invert aeromagnetic and satellite magnetic field data sets for crustal magnetizations (e.g., [65]), involves determining the size of the three vector components of the moment of each of the dipoles in the grid. The positions of the *N* dipoles were fixed while their individual moments and directions were allowed to vary, so that 3*N* parameters were solved for. Our inversions were implemented in MATLAB on a Sun Ultra 10 workstation. The UHRSSM data taken over several different regions of 227b were taken as subsets and an inversion was performed individually on each subset. Examples of two such inversions are presented in Fig. 3.9. For each of the data subsets, we performed the equivalent source scheme twice, once using conjugate gradient analysis (a sparse matrix method which takes advantage of the rapid decay of dipole magnetic fields with distance) [66], and then again using truncated singular value decomposition [67]. Both approaches solve for the smallest possible normed magnetization consistent with the field data, and both yielded similar magnetization solutions.

The inversions (e.g., Fig. 3.9) confirm that carbonates, chromite, and fusion crust are the source of magnetic fields observed above our samples. The inversions (Fig. 3.9) also demonstrate that regions of the 227b thin section rich in carbonate-bearing magnetite and pyrrhotite (e.g., Fig. 3.8h,m) have magnetizations of ~0.1 to 1.6 A/m. Given the fractional abundance of carbonate in these regions, this would suggest that the carbonates have magnetizations of a few A/m. A small patch of carbonate in 227b has been disaggregated and transported by melted

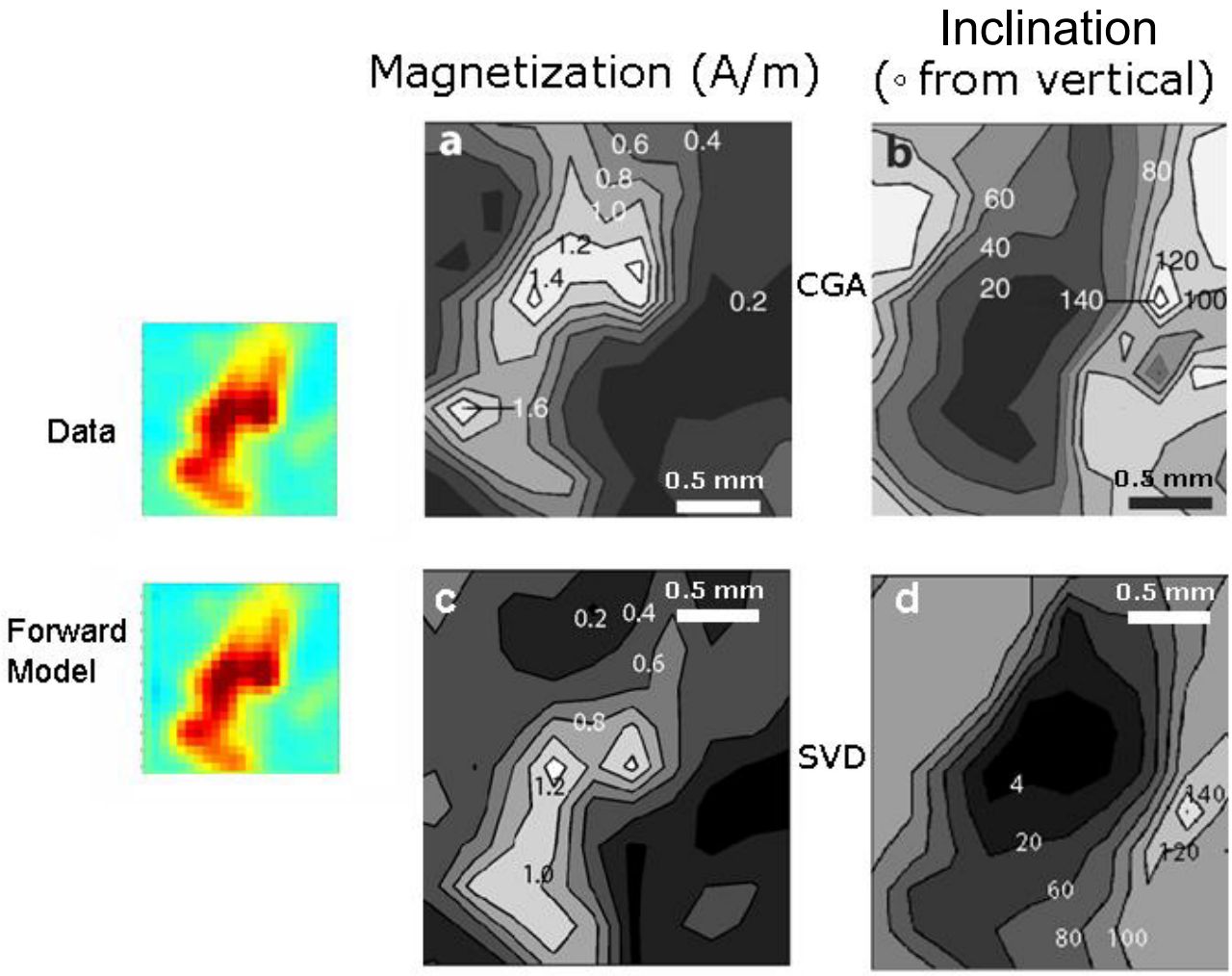

Fig. 3.9 Magnetization inversions of UHRSSM data from a selected portion of ALH84001,227b,1. Data are taken from dashed boxed region of Fig. 3.8. The least squares solutions were obtained with an equivalent source scheme solved by **a,b**) conjugate gradient analysis (CGA) and **c,d)** truncated singular value decomposition (SVD). The data are reproduced at top left and the forward model (calculated using fitted parameters from conjugate gradient analysis) are shown at bottom left. A grid of $N = 144$ regularly spaced dipoles was used, and the total number of UHRSSM measurements in the boxed region was 576. **a,c)** Contour plots of magnetization (A/m). **b,d)** Contour plots of inclination of magnetization, where 0◦ is oriented directly upwards and 90◦ is in the plane of the thin section. The contour lines in (a,c) are 0.2, 0.4, 0.6, 0.8, 1.0, 1.2, 1.4, and 1.6 A/m, with brighter regions having larger values. The contour lines in (b,d) are 4◦, 20◦, 40◦, 60◦, 80◦, 100◦, 120◦, and 140◦, with brighter regions having larger values. The scale bars are 500 μm. Because in these inversions we did not take into account the finite size of the UHRSSM's pickup coil (which has a diameter of 250 μm = 2.5 pixels), the actual size of the strongly magnetized region in the center-bottom of (a) should be ~1-2 pixels smaller in both the horizontal and vertical directions.

feldspathic glass (Fig. 3.8f,l,m), during which its magnetization direction (Fig. 3.8e) appears to have rotated with respect to that of carbonates elsewhere in the thin section (Fig. 3.8c). This change in direction probably resulted from thermal remagnetization of the carbonate due to heating within the hot glass, although it may have also been partly the result of physical rotation of the carbonate. A less likely possibility is that the carbonates formed over a period of time during which the absolute orientation of the local magnetic field changed. It is clear from our magnetization inversions (e.g., Fig. 3.9) that carbonates, although locally magnetized in a single direction (as in the case of the patch of carbonate at the bottom of Fig. 3.8c), are as a whole magnetized in at least three different directions: compare orientations of dipoles associated with carbonates in Figs. 3.1b and 3.8c,e.

Chromite grains are volumetrically more abundant than carbonate in 227b by at least an order of magnitude, but only in some cases have a detectable magnetic signature (Fig. 3.8a,b,e,f,j). Although stoichiometric chromite ($FeCr_2O_4$) is paramagnetic at room temperature, Mg- and Al-rich chromites similar to those in ALH84001 (which have a mean composition of roughly $Fe_{1.05}Cr_{1.31}Al_{0.35}Mg_{0.20}Ti_{0.06}O_{4.0}$) [68] have been found to have Curie points above 300◦C [69, 70]. Furthermore, no exsolution lamellae have ever been identified in the ALH84001 chromites (despite searches for them [44]), suggesting that the magnetization in the chromites may be intrinsic to these phases rather than originating from intimately exsolved magnetite. The anomalies associated with the chromites in ALH84001 are approximately dipolar, with orientations in at least two and possibly three different directions. There are at least three westwardly magnetized chromites in Fig. 3.8a and an eastwardly one in Fig. 3.8e, while the second and third labeled chromites from left in Fig. 3.8a could be unidirectionally magnetized in a third direction. Thus, much of the spatial

heterogeneity of magnetization observed previously [5, 18, 20] is the signature of carbonate and chromite magnetized in multiple directions.

5. Thermal Constraints on the Carbonate

There is considerable debate about whether carbonates in ALH84001 were heated during or after their formation at 4 Ga [15, 64, 71-74]. This is critical because determining the age of the magnetization in the carbonates requires knowing the last time they were heated above the Curie point of magnetite (580°C at a pressure of 1 bar). Even brief (<<1 s) excursions above the Curie point would be sufficient to completely remagnetize the meteorite.

One of the most likely processes that heated the meteorite is shock resulting from impacts on the martian surface. As discussed in Section 1, ALH84001 has clearly been affected by multiple shock events [15, 23, 55]. However, despite their high peak temperatures, these shocks did not necessarily remagnetize the meteorite. This is because the pressure dependence of magnetite's Curie point has never been measured for high pressure shocks. In fact, if the very steep rise of the Curie point with pressure (20°C GPa^{-1}) that has been measured at hydrostatic pressures up to 0.6 GPa [75] continues to hold true at higher shock pressures, this would suggest that the peak temperatures produced during shocks might not completely remagnetize rocks. In that case, only shocks with post-shock temperatures exceeding the Curie point would be capable of remagnetizing rocks. A second caveat is that it is probable that like most shocked rocks, ALH84001 has been heterogeneously deformed and heated by the shock events it has experienced (see Section 6). Given that at least one and possibly multiple shocks occurred after formation of the carbonates (see below), this means that some carbonates probably have been significantly

heated one or more times while others may have experienced fewer or even no heating events. For the purposes of dating the magnetization in the carbonates, we will consider both possibilities: carbonates that may have been heated and those not heated since they formed.

Petrographic studies [15] have identified one major shock event that occurred after the formation of the carbonates. This is confirmed by our SEM and X-ray spot analysis data on the carbonate in slice 232e (Fig. 3.1a) and 227b (Fig. 3.8d,f,h,i,k), which demonstrate that like many ALH84001 carbonates, it is adjacent to anhedral feldspathic glass. This glass, which has been observed elsewhere in the meteorite [15, 23, 55] and lacks even short-range order [15, 76], does not retain the shape of a relict feldspar crystal, is unfractured (unlike its immediate surroundings), fills irregular cracks and voids in the pyroxene, and even occasionally intrudes and disaggregates carbonate (see Fig. 3.8f,l,m and [23]). All of these observations indicate that the glass in our samples and throughout ALH84001 was melted and mobilized one or more times (the last such event was labeled "D3" by Treiman [15]). Because microfaults in the 232e carbonate do not extend into the adjacent glass (Fig. 3.1a) and the glass occasionally intrudes 227b carbonate (Fig. 3.8l,m), it appears that at least some of the glass melted after the carbonates formed. Because the glass was hot enough to flow during this event, the intruded carbonate and any nearby material probably experienced a shock with peak pressures of 40 to 60 GPa [15, 77] and post-shock temperatures of 400 to 1000°C [77, 78]. These post-shock temperatures should have remagnetized most of the magnetite and pyrrhotite adjacent to the melted glass.

On the other hand, several geochemical studies of oxygen isotope and cation gradients in ALH84001 indicate that other, unfractured carbonates have not been significantly heated since they formed at 4 Ga [71, 79]. Textural studies have documented rare patches of feldspar in ALH84001 that retain the outline of a

feldspar crystal [15, 80], have relic twins or cleavage [15], and/or are crystalline [80]. The geochemical data could be reconciled with the evidence for a high temperature glass flow event if the meteorite cooled quickly following that event. Both the geochemical and textural data also permit a late shock event that heterogeneously affected the rock, leaving isolated regions unheated and undeformed. Shock heterogeneity [81, 82], in concert with brecciation and associated rotation of carbonates, would also help to explain why the carbonate minerals are locally (on a scale of several mm and less) magnetized in the same direction (Fig. 3.8c) but are as a whole (on a scale of cm or more) magnetized in multiple directions (compare Figs. 3.1b and 3.8c,e).

To resolve these issues, we have used data from $^{40}Ar/^{39}Ar$ dating of ALH84001 feldspathic glass to place an upper limit on the temperatures it and nearby carbonates have experienced during the last 4 Gyr. Several different laboratories have shown that the meteorite's $^{40}Ar/^{39}Ar$ chronometer was last reset sometime between 3.9 and 4.3 Ga [33, 83]. Unfortunately, these dates are statistically indistinguishable from the Rb/Sr and Pb/Pb ages of the carbonates (3.90 ± 0.04 Ga and 4.04 ± 0.1 Ga, respectively) [14], and so do not by themselves specify whether the carbonates formed before or after the $^{40}Ar/^{39}Ar$ chronometer was reset. Using thermochronological modeling of several limiting thermal histories of the meteorite, we have demonstrated in Chapter 4 [84] that most of ALH84001 feldspathic glass has not been heated ~<350 to 500°C and shocked to peak pressures ~<1 GPa since the glass was last melted. This indicates that most of ALH84001, including carbonate associated with the glass, has not been above these temperatures since 3.9-4.1 Ga.

6. The Age of the Magnetization in ALH84001

Any magnetite and pyrrhotite in carbonates heated during the last glass-melting event should therefore retain thermoremanent magnetizations that originated during that event. The magnetization of such carbonates must then have been acquired at 3.9-4.1 Ga (using the youngest possible $^{40}Ar/^{39}Ar$ date [33] as a lower limit on the age of the magnetization and the oldest date on the carbonates [14] as an upper limit). Because the shock at 4 Ga produced very high and long-lived post-shock temperatures (see above and Chapter 4), any phase transitions that occurred during the shock itself are unlikely to have left metastable or otherwise nonthermal remanent magnetization (e.g., [51, 85]) in the carbonates.

Any carbonates not heated during the last glass-melting event would retain nearly all of their magnetization acquired at the time of their formation at ~3.9 to 4.1 Ga. The latter carbonates could have a depositional, crystallization, or thermoremanent magnetization. That pyrrhotite and magnetite in ALH84001 carbonate have probably not been shocked ~>1 GPa since 4 Ga (Chapter 4 and [84]) means that they have not since been subject to shock-induced magnetization changes and phase transitions (occurring at pressures of >1 GPa and >1.6 GPa for magnetite and pyrrhotite, respectively [51, 85]), which might otherwise alter their primary 4 Ga remanence. In summary, our results permit some carbonates to have been affected by localized heating since their formation. However, in most cases any such localized heating must have occurred very soon after their formation.

Our data show that most of the carbonates in ALH84001 should retain magnetizations they acquired at 3.9 to 4.1 Ga on Mars. Depending on their Curie points and rock magnetic properties, chromites located near feldspathic glass could retain a magnetization at least this old. Because chromites are believed to be primary igneous minerals in ALH84001, some of their magnetization could in

fact be as old as the meteorite's crystallization age, 4.5 Gyr. On the other hand, the magnetization in the chromites may not have been acquired in a magnetic field (if the magnetization is simply the result of zero-field alignment along an easy axis) or else it could have been acquired in a field more recently (if the chromites have low Curie points and/or easily acquire viscous remanence). The fact that chromites are magnetized in different directions is consistent with zero-field remanence, but also with a scenario in which the chromites have experienced a range of thermal histories and/or have been rotated during one or more brecciation event since their formation. In the latter scenario, various grains may have reached temperatures exceeding their magnetic blocking temperatures at different times between 4.5 and 4.0 Ga, during which the relative orientation of the local magnetic field changed.

Such a heterogeneous thermal and deformational history is supported by textural observations that chromites within cataclastic granular bands of orthopyroxene (which contain many carbonates and so must predate 4 Ga) have been severely deformed into elongate anhedral stringers (e.g., chromite adjacent to carbonates at bottom of Fig. 8d), while chromites located outside these granular bands are rarely subhedral and less fractured (Fig. 8b,f). Additional evidence that some chromite may have escaped late heating comes from the identification of two regions in ALH84001 with $^{40}Ar/^{39}Ar$ laser probe ages of 4.4 Ga [83]. Determining the exact age and origin of the magnetization in the chromites will require a detailed analysis of their magnetic properties combined with low blocking temperature geochronometers capable of placing thermal constraints directly on individual chromite grains.

7. Implications for the Timing of the Martian Dynamo

The magnetization in ALH84001 carbonates is the oldest ever identified in any planetary rock and the only well-dated remanence in a martian sample. It is at least 400 Myr older than the oldest magnetization identified in an Earth rock [86]. We have shown (Section 3) that a typical ALH84001 zoned carbonate is composed of ~1 wt% pyrrhotite and magnetite in a mass ratio of ~0.3 to 0.5, and these are SD (~70%) and SP (~30%) in size [19]. Thus, the carbonates in ALH84001 should have a saturation IRM of ~10^3 A/m. Since our magnetization inversion demonstrates that the carbonates have NRMs of a few A/m (e.g., Fig. 9) we estimate that the ratio of their NRM to their IRM is ~0.1 to 1%. This estimate roughly agrees with the NRM to IRM ratios of ~3% directly measured for each of three bulk grains taken from the interior of ALH84001 [18] (the magnetization of such grains is likely to be dominated by any interior carbonates). A thermoremanent magnetization acquired by single domain magnetite grains in a field of 50 μT will generally be a few percent of IRM, while detrital remanence produced in the same field will be ~0.1% of IRM [87, 88]. Thus, the NRM to IRM ratios of ALH84001 samples are consistent with an origin as a thermoremanent (detrital remanent) magnetism in a field roughly 0.1 to 1 times (1 to 10 times) that at the surface of the present-day Earth. These values may be lower limits given the heterogeneous orientation of the magnetization in the meteorite (Figs. 3.7 and 3.8), and should be reproduced with more robust paleointensity experiments like that of Thellier-Thellier [62]. This magnetizing field would be adequate for magnetotaxis by the bacteria whose magnetofossils have been reported in ALH84001 [19], and may have been capable of producing the intensity of the magnetic anomalies [45] on the martian surface.

Such a field is unlikely to have been that of the Sun, the solar wind, or other planets, whose total intensity is not thought to have been much larger than the

present value (several nT) at Mars' current orbit 4 Ga [40]. Fields generated or amplified by impact-produced plasma [89, 90] have never been conclusively demonstrated to occur in nature [91]. A simpler explanation is that ALH84001 was magnetized by either a martian geodynamo or by local crustal remanent fields like those in the martian southern hemisphere [45]. Since a martian geodynamo field presumably produced the crustal magnetizations, our data imply that Mars had a magnetic field generated by an active geodynamo by at least 4 Ga. It is not clear if the dynamo still remained active at 4 Ga. This agrees with but is much more precise than the crater count ages (3.0-4.5 Ga, and most probably >3.7 Ga) [92] inferred for the surfaces associated with the martian crustal magnetizations. Our data do not support recent suggestions [46] that the martian dynamo originated substantially after the formation of the large impact basins. Instead, our results are consistent with thermal evolution models of Mars that predict a convecting core and geodynamo extending from 4.55 Ga (or possibly delayed by several hundred Myr) to sometime after 4 Ga [93-97]. Because we are unable to determine whether the martian dynamo was still active at 4 Ga, our results do not directly constrain the age of Hellas or other unmagnetized impact basins situated within the crustal magnetic anomalies. Given that chromites in the meteorite could retain a magnetic remanence that predates that of the carbonates, ALH84001 may contain records of martian fields older than 4 Ga, possibly even dating back to near the time of planetary formation.

8. Summary

In Chapter 3, we have demonstrated the following:

1. Magnetite and pyrrhotite within carbonates carry much of the magnetization in the interior of ALH84001.

2. The carbonates were magnetized prior to ~3.9 Ga.

3. The intensity of their magnetization gives evidence that a martian dynamo was active at or prior to ~3.9 Ga.

4. The magnetization intensity implies a magnetic field on Mars of intensity within an order of magnitude of that at the surface of the present-day Earth.

5. Chromite in ALH84001 also retains a magnetization of unknown origin, stability, and age.

Chapter 4

TEMPERATURES ON MARS FROM $^{40}Ar/^{39}Ar$ THERMOCHRONOLOGY OF ALH84001[4]

The thermal history of martian meteorite ALH84001 has critical implications for its petrological and deformational history, the age of its trapped atmospheric gases, the timing of the martian dynamo, and possibly the evolution of martian surface temperatures during the last 4 billion years (Gyr). Feldspathic glass in ALH84001 has been dated using $^{40}K/^{40}Ar$ and $^{40}Ar/^{39}Ar$ chronometry by several laboratories. There is general agreement that these chronometers were last reset sometime between 3.9 and 4.3 billion years ago (Ga). Using the $^{40}Ar/^{39}Ar$ data from Bogard and Garrison (1999) to model several limiting thermal histories of the meteorite, here we show that most of ALH84001 feldspathic glass has probably not been heated to more than ~350 to 500◦C and shocked to peak pressures of ~<1 GPa since the glass was last melted. ALH84001 has also not been shocked to peak temperatures more than a few ◦C above ambient since this time. This indicates that most of ALH84001 has been well below these temperatures since 3.9 to 4.3 Ga. Since these temperatures are below the Curie point of magnetite, much of the magnetization we identified in ALH84001 carbonate (see above) must have been acquired by ~4 Ga. This also provides an explanation for why ALH84001 contains a sample of an apparently ancient martian atmosphere that is less evolved relative to that on present-day Mars. Our calculations also suggest that for the last 4 Gyr,

---

[4] Adapted from: Weiss, B. P., D. L. Shuster, S. T. Stewart (2002) Temperatures on Mars from $^{40}Ar/^{39}Ar$ thermochronology of ALH84001, *Earth Planet. Sci. Lett.*, **201**, 465-472.

average surface temperatures on Mars may not have been much higher than the present cold conditions.

1. Introduction

The meteorite ALH84001 is an orthopyroxene cumulate from Mars with a Sm/Nd age of 4.50 Ga [12, 98]. This extreme age—the oldest known for any planetary rock—is reflected by the multiple episodes of intense deformation recorded by the meteorite's petrofabric [15]. During the first few hundred million years of its history, ALH84001 was partially melted and fractured by several shock events. In some of these fractures formed zoned carbonate blebs with Rb/Sr and Pb/Pb ages of 3.90 ± 0.04 Ga and 4.04 ± 0.1 Ga, respectively [14] (although the Rb/Sr dates are controversial [53]). Feldspathic glass, which makes up ~1 wt% of the meteorite, is ubiquitously distributed throughout the rock and very commonly surrounds carbonates [15]. The texture, shape, and structure of this glass indicate that it was shocked and mobilized (and probably melted) at least once after the carbonate formed[7, 15, 23, 55, 99]. The last such event was labeled "D3" by Treiman [15], during which ALH84001 apparently experienced peak pressures of 40 to 60 GPa [15, 77] and post-shock temperatures of 400 to 1000°C [77, 78, 99].

Several laboratories have conducted $^{40}K/^{40}Ar$ and $^{40}Ar/^{39}Ar$ dating of ALH84001 using stepped heating of bulk grains [16, 26, 33, 83, 100, 101] and by laser probe [83]. Essentially all experimenters agree that the dominant carrier of K and radiogenic ^{40}Ar in ALH84001 is feldspathic glass. There is also near universal agreement that the meteorite last completely degassed ^{40}Ar sometime between 3.9 and 4.3 Ga (depending on the composition assumed for trapped Ar). On the other hand, laser probe dating [83] has identified a few

locations in the meteorite having $^{40}Ar/^{39}Ar$ ages of 4.4 Ga. This suggests that while much of the meteorite was strongly heated sometime during 3.9 to 4.3 Ga, isolated locations may have escaped heating since 4.4 Ga, possibly due to the spatially heterogeneous nature of shock heating [82]. The coincidence of the main ~4 Ga population of $^{40}Ar/^{39}Ar$ ages with those of impact glasses from the lunar highlands provides the first direct evidence that Mars may have experienced a heavy bombardment of impactors contemporaneous with the lunar cataclysm [102].

Here we demonstrate that the $^{40}Ar/^{39}Ar$ chronometer of ALH84001 was probably last reset by the D3 shock event that mobilized its feldspathic glass. This was presumably the result of an impact on the martian surface. We show that ever since this time, the meteorite has experienced very mild temperatures and shock pressures.

2. Thermochronology

Using the ^{39}Ar release data of Bogard and Garrison [33], we modeled (following the methods of [103]) the temperature dependence of the diffusion coefficient of Ar through ALH84001 feldspathic glass using an Arrhenius relationship, $D(T) = D_0/a^2 \exp(-E_a/RT)$, for characteristic constants D_0/a^2, E_a, and the gas constant R (Fig. 4.1). From this we derive best fit values of $\ln(D_0/a^2) = -1.9 \pm 0.2$ $\ln(s^{-1})$ and $E_a = 76.8 \pm 1.3$ kJ mol^{-1} (these uncertainties are formal errors from the regression analysis only), with a linear correlation coefficient $r^2 = 0.998$ (number of heating steps $n = 12$). In the calculations presented below, we assume that this Arrhenius relationship has held for ALH84001 glass since it was last mobilized during the D3 deformational event and that the diffusion domain size a is constant for all time in our calculations.

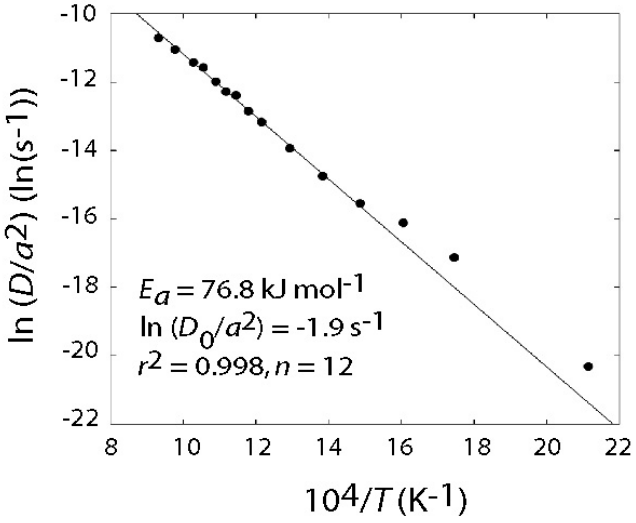

Fig. 4.1 Arrhenius plot for ALH84001,113. Shown is the calculated temperature dependence of the diffusion coefficient of ^{39}Ar through ALH84001 feldspathic glass, $D(T)$. Spherical diffusion domain geometry was assumed. Plotted is the natural logarithm of the ratio of D to the squared diffusion domain radius, a^2, as a function of inverse temperature. Data were taken from the stepwise heating experiments of Bogard and Garrison [33] up to the 850◦C step. The solid line is our best-fit Arrhenius relationship excluding the three low temperature points (see text for discussion), which has an ordinate-intercept of $\ln(D_0/a^2)$= -1.9 ± 0.2 $\ln(s^{-1})$, a slope of E_a = 76.8 ± 1.3 kJ mol^{-1}, and a linear correlation coefficient r^2 =0.998.

Because ^{39}Ar resides in several distinct phases [33], we used ^{39}Ar released only from the high K/Ca phases (i.e., the 200 to 850◦C steps) in our calculation of $\ln(D/a^2)_i$ for each step i (Fig. 4.1). Following the conclusions of Bogard and Garrison [33] and Turner *et al.* [83], we assume that ^{39}Ar released during steps >850◦C (which presents as anomalously low ages in the age spectrum between 80 and 92% cumulative gas release; see Fig. 4.2) is the product of recoil, and so we excluded these from the regression (Fig. 4.1). We also excluded the three steps <450◦C from the regression (Fig. 4.1) because some of that gas was possibly derived from a recently precipitated weathering product [33]. Inclusion of the latter values in the regression would have a negligible effect upon our conclusions.

The Arrhenius relationship is more sensitive to which steps we include in our calculation of $\ln(D/a^2)$ [103]. For instance, if we exclude the steps <450◦C from the calculation, our best-fit values become $\ln(D_0/a^2) = 1.3 \pm 0.4$ $\ln(s^{-1})$ and $E_a = 103 \pm 2.6$ kJ mol^{-1}. In their $^{40}Ar/^{39}Ar$ experiments on ALH84001, Turner *et al.* [83] obtained a similar value for E_a and also noted its dependence on the low temperature release. We do not favor the latter values since they rely on less of the measured data: the latter calculation entirely ignores the first three release steps, requires excluding three high temperature steps from the regression to maintain reasonable linearity, and provides a poorer fit to the resulting regression ($r^2 = 0.995$; $n = 9$).

Our goal is to determine the maximum temperature the meteorite experienced during the last 4 billion years (Gyr). The primary observational limit is the fraction of "missing" radiogenic ^{40}Ar that has been diffusively lost from the feldspathic diffusion domain(s). To quantify this fraction, we forward modeled the distribution of Ar in the glass using the previously derived Arrhenius relationship (Fig. 4.1). We assumed the idealized case of a uniform size distribution of spherical diffusion domains containing a uniform distribution of ^{39}Ar (produced from experimental irradiation of K) but which had recently (within the last few million years) diffusively lost some fraction (1%, 5%, or 10%) of the total ingrown ^{39}Ar. We then put these grains through a simulated stepwise heating schedule. Based on the diffusion parameters determined from Bogard and Garrison's [33] data (discussed above) and the same heating schedule of their experiment, we calculated the expected $^{40}Ar/^{39}Ar$ ratio as a function of cumulative ^{40}Ar release fraction. A comparison of the model results with the

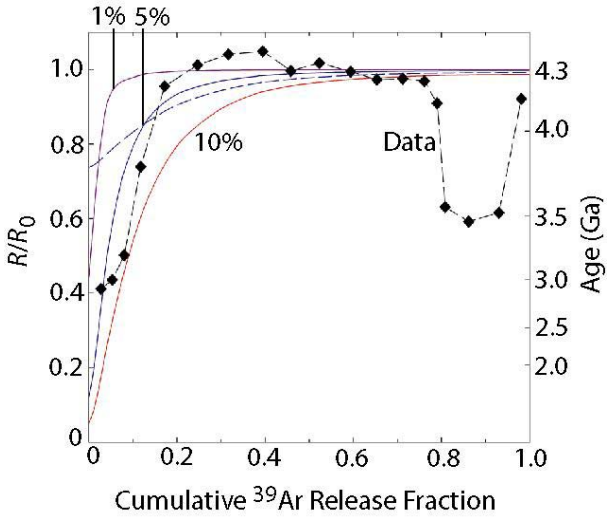

Fig. 4.2 Model age spectra compared to data. Shown is the $^{40}Ar/^{39}Ar$ ratio, R (normalized to the ratio at the center of the diffusion domain, R_0), plotted as a function of cumulative ^{39}Ar release fraction. Age spectra were calculated for various degrees of diffusive ^{40}Ar loss and a uniform distribution of ^{39}Ar. Also plotted is the $^{40}Ar/^{39}Ar$ spectrum for ALH84001,113 measured by Bogard and Garrison [33], normalized to the $^{40}Ar/^{39}Ar$ ratio of the mean plateau age of 4.3 Ga. Included are the $^{40}Ar/^{39}Ar$ ages reported in [33] for reference. The color of each solid curve corresponds to a different amount of radiogenic ^{40}Ar lost at 15 Ma (expressed as a fraction of the total amount of initial radiogenic ^{40}Ar): purple = 1% lost, blue = 5% lost, red = 10% lost. For comparison, we include the expected release pattern for 5% lost ^{40}Ar, assuming instead that the loss event occurred at 3.5 Ga ago and was followed by 3.5 Gyr of quantitatively retained radiogenic ingrowth (dashed blue curve).

measured ratios (Fig. 4.2) demonstrates that curves corresponding to ≥5% gas loss (solid blue and red curves) reach a plateau at significantly higher cumulative release fractions than do the data (black diamonds). This conclusion is insensitive to the choice of age to which the data are normalized. We conclude that <5% missing ^{40}Ar fraction most closely matches the observations. A similar result is obtained if diffusive loss of ^{40}Ar had instead been assumed to occur 3.5 Ga and had been followed by 3.5 Gyr of radiogenic ingrowth (Fig. 4.2, dashed blue curve).

Before continuing, we discuss the sensitivity of this conclusion to the imperfections in the age spectrum. Firstly, the three points with cumulative ^{40}Ar

release between 80 and 92% (age ~3.5 Ga) in Fig. 4.2 are thought to reflect a recoil effect due to the juxtaposition of a K-rich and K-poor phase [33]. The above conclusions drawn from Fig. 4.2 are therefore based on the comparison between our model and the $^{40}Ar/^{39}Ar$ observations for cumulative release fractions less than ~80%. Secondly, although some ^{40}Ar may have been inherited by ALH84001 as a result of weathering in Antarctica, much of the ^{40}Ar from the outer regions of the feldspar diffusion domains was almost certainly lost to surrounding pyroxene during recoil [33]. For this reason, we conservatively estimate that less than 5% of the total ^{40}Ar in the meteorite has been lost since the $^{40}Ar/^{39}Ar$ chronometer was reset. This places stringent limits on the amount of heating that ALH84001 can have experienced since 4 Ga.

We used the Ar release data of Bogard and Garrison [33] to estimate the amount of gas that would be lost during several hypothetical thermal histories. Given the lack of geologic and historical context for the meteorite, we first examined the most stringent scenario, in which the meteorite (approximated as a sphere with a preatmospheric radius of ~0.2 m [26, 104]) was exposed to an elevated temperature T_0 near the time of its ejection from Mars 15 million years ago (Ma). We assumed that only the meteorite's volume was instantly heated to T_0 while its surroundings remained initially at ambient martian surface temperatures (~210 K). We then calculated the central temperature of the rock as a function of time while it conductively cooled, using one of two different thermal boundary conditions. Firstly, to approximate cooling during shallow (<1 km) burial in the regolith, we assumed an infinite surrounding medium of composition similar to the meteorite and initially at 210 K. Secondly, to approximate cooling in space or on the martian surface, we assumed a Stefan-Boltzmann radiative boundary condition at the meteorite's surface (taking an emissivity of ~0.93 and a solar insolation equilibrium temperature of 210 K),

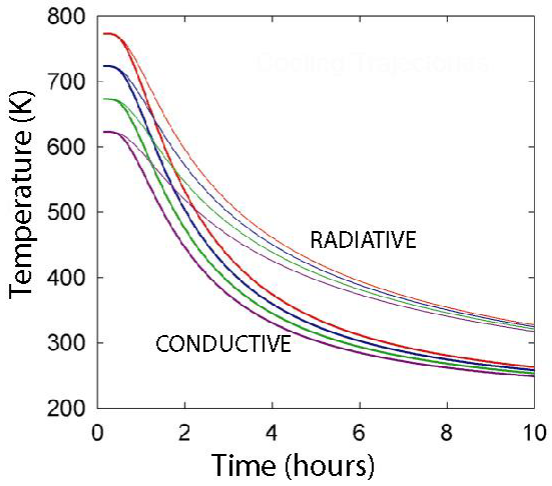

Fig. 4.3 Thermal diffusion calculations. Shown is the temporal evolution of the central temperature of ALH84001 during cooling from several initial temperatures. The color of each curve corresponds to a specific initial pulse temperature T_0: red = 500◦C, blue = 450◦C, green = 400◦C, and purple = 350◦C. The bold and fine curves were calculated assuming a conductive and a radiative boundary condition, respectively (see text).

with conductive heat transport in its interior. For these calculations, we used a thermal diffusivity of 10^{-6} m^2 s^{-1}, a specific heat of 815 J kg^{-1} K^{-1}, and a density of 3300 kg m^3, typical of $MgSiO_3$. The conduction-only scenario has an analytic solution [105], while the combined conduction-radiation scenario required numerical integration of the diffusion equation. Under both boundary conditions, the meteorite cools at roughly the same rate to near ambient temperatures within a couple of days (Fig. 4.3).

Such fast cooling prevents calculation of a meaningful closure temperature for Ar diffusion using Dodson's method [106]. As a result, we directly modeled the effects of a thermal pulse on the Ar content of ALH84001. For each of these thermal boundary conditions, the measured ^{40}Ar diffusion parameters, and for

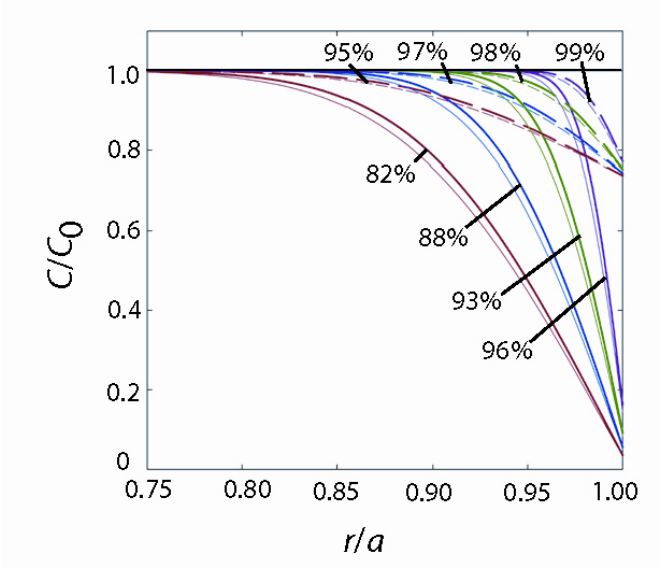

Fig. 4.4 Radial Ar distribution profiles following heating. Shown is the calculated radial distribution of radiogenic ^{40}Ar in spherical ALH84001 feldspar diffusion domains after the meteorite cooled from various starting temperatures (Fig. 4.3). Shown is the ^{40}Ar concentration, C (normalized to the initial concentration at the center of the diffusion domain, C_0), at various radial distances from the center of the diffusion domain, r (normalized to the radius of the domain, a). For these calculations we have assumed an initially uniform distribution of ^{40}Ar prior to the thermal pulse. The solid and dashed curves were calculated assuming the thermal pulse occurred at within the last few million years and at 3.5 Ga, respectively. Bold and fine curves were calculated assuming a conductive and a radiative boundary condition, respectively. The color of each curve corresponds to a specific initial pulse temperature T_0: red = 500°C, blue = 450°C, green = 400°C, and purple = 350°C. The initial gas distribution prior to heating is shown by the solid horizontal black line. The colored curves were calculated by inputting the corresponding thermal history (Fig. 4.3) into an Ar diffusion program (adapted from the (U-Th)/He thermochronology code of Wolf *et al.* [107]). The number next to each thick line is the total fraction of remaining ^{40}Ar in the grains (i.e., integral of the radial fraction of gas over the entire grain volume) following cooling under the conductive boundary condition.

several different values of T_0, we calculated the radial distribution of ^{40}Ar remaining after the rock had cooled to ambient martian surface temperatures. These computations were implemented using a program adapted from a (U-Th)/He thermochronology code developed by Wolf *et al.* [107]. We assumed a uniform size distribution of spherical feldspathic grains each containing an initially spatially uniform distribution of ^{40}Ar and with the thermal diffusivity as measured (Fig. 4.1). Compared to a uniform distribution of grain sizes, a

lognormal distribution of the same mean and with a variance of 0.4 to 0.6 (the best-fit size distribution found by Turner *et al.* [83]) will require slightly less (but nearly identical) time to degas the small amounts (<10%) of total ^{40}Ar considered here [108]. Because no more than ~5% of the gas in the meteorite can be lost during the thermal pulse (Fig. 4.2), these calculations (solid curves in Fig. 4.4) demonstrate that the maximum temperature of the thermal pulse at 15 Ma is ~350◦C. If we move the hypothetical thermal pulse back to an earlier time in the meteorite's history, there will be less ^{40}Ar available to be degassed, and so higher values of T_0 for earlier thermal events are consistent with the 5% loss criterion. In particular, our calculations show that thermal pulses with T_0 > 400◦C at 2 Ga will also lead to >5% ^{40}Ar loss, as will pulses with T_0 > 500◦C at 3.5 Ga (dashed curves in Fig. 4.4). These results are not sensitive to the method by which we calculated the Arrhenius relationship (e.g., whether or not we included the first three temperature steps in calculating D/a^2).

These are upper limits on the temperatures that ALH84001 has experienced during the last 4 Gyr for several reasons. Firstly, if we had instead assumed that a volume of rock larger than the meteorite was heated to T_0, the cooling time (and therefore ^{40}Ar loss) would be larger (and the maximum temperature lower) than that estimated here. Secondly, we neglected the very significant ^{40}Ar loss that the meteorite experienced while at equilibrium temperatures during its 4 Gyr residence on Mars, 15 million years (Myr) in space, and 11,000 years on Earth. It is difficult to estimate precisely how much additional gas was lost during these periods, during which the meteorite's temperature history is not precisely known. A second difficulty comes from the likelihood that the temperatures experienced during much of these periods were several hundred ◦C below those for which the Arrhenius coefficients were measured [33, 83]. Nevertheless, using a linear extrapolation of the derived Arrhenius relationship (Fig. 4.1), we estimated the amount of ^{40}Ar that should have been degassed from the meteorite during the last

15 Myr in space and on Earth. We found that, depending on the orbital path taken by the meteorite from Mars to Earth, the Ar loss could have been anywhere from ~4% (in the limiting scenario in which the meteorite spent nearly all of the last 15 Myr at or beyond Mars' orbit) to several tens of percent or more (if it spent more of this period at smaller semimajor axes). Because the meteorite has lost less than 5% of its ^{40}Ar (Fig. 4.2), this strongly suggests that the actual maximum temperature experienced by the meteorite during any conductively cooling thermal pulse in the last 4 Gyr is well below (conceivably several hundred ◦C below) our nominal 350 to 500◦C limit.

We now consider the possibility that ALH84001 was heated sometime in the last ~4 Gyr by a high temperature shock event. Much (but usually not all) of the temperature rise that occurs during a shock can cool adiabatically much faster than a conductively cooling thermal pulse to the same peak temperature [32]. In any case, ALH84001 probably has not been significantly shock-heated because the feldspathic glass in the meteorite is very rarely fractured. The lack of fractures requires that since it was last melted, the glass could not have been differentially stressed at pressures exceeding its tensile strength (~1 GPa) [109, 110] unless it reached pressures sufficient for the production of diaplectic glass (~30 to 35 GPa) [77]. However, such pressures would be associated with post-shock temperatures exceeding ~250◦C [77]. Since the meteorite would then have to conductively cool from these post-shock temperatures, our previous conductive calculations render them (and the shocks that produce them) unlikely. There is also no other textural or petrological evidence in the meteorite for any shock events younger than the last glass flow event [15]. This means that most of ALH84001 probably has experienced negligible shock-heating (no more than several ◦C above ambient temperatures) since this event.

3. Implications

The glass and any nearby carbonates probably have not experienced peak shock pressures above ~1 GPa and temperatures above ~350 to 500◦C for even very short time periods during the last 4 Gyr. ALH84001 was also not shock-heated to more than a few ◦C above ambient Martian surface temperatures during ejection. Since these temperatures are below the Curie point of magnetite, much of the magnetization measured in ALH84001 carbonates intimately associated with the glass (see Chapters 2-3 and [54]) must have been acquired by ~4 Ga. This provides independent verification of the conclusions of Chapter 2 and [5] (and the breccia test by Kirschvink *et al.* [18]) that ALH84001 was not heated above ~40◦C during the last 15 Ma. This also provides an explanation for why the isotopic composition of martian atmospheric Xe, N, H, and Ar trapped in ALH84001 resembles that expected for an atmosphere less evolved than that presently on Mars [28, 34, 111-116] (see Table 4.1). Given that a shock of at least several tens of GPa is probably necessary for shock-implantation of the large amount of atmospheric gases in ALH84001 [117, 118], our results strongly support suggestions [28, 34, 111-116] that the meteorite contains a sample of 4 Gyr old martian atmosphere. That these gases are enriched in light isotopes of H and N relative to present-day values (Table 4.1) supports the hypothesis that significant atmospheric loss has occurred on Mars since 4 Ga.

Given the very high and probably long-lived post-shock temperatures that followed the glass-mobilization D3 event, our diffusion calculations suggest that it was responsible for resetting the $^{40}Ar/^{39}Ar$ chronometer throughout most of the meteorite at ~4 Ga. That the D3 event (and not an earlier deformational event) was capable of resetting the chronometer is also supported by the lack of

Measurements of Martian Atmospheric Gases

	ALH84001 (4 Ga)	EETA79001 (0.18 Ga)	Viking (present)
D/H	**3 x**	5.4 x	5.5 ± 0.25 x
$^{15}N/^{14}N$	**1.007 x**	<1.50 x	1.62 ± 0.16 x
$^{129}Xe/^{132}Xe$	**2.16**	2.4-2.6	2.3-2.6
$^{36}Ar/^{38}Ar$	**≥ 5**	≤ 3.9	5.5 ± 1.5
$^{40}Ar/^{36}Ar$	**≤ 128**	~1800	3000 ± 500

x = times Earth's atmospheric ratio

Data summarized by Bogard *et al.* 2001
(See papers by Sugiura, Marti, Mathew, Marty, Gilmour, Grady, Eiler, Garrison, Murty…)

Table 4.1 Measurements of martian atmospheric gases. Shown are gases trapped in the 4 Gyr old martian meteorite ALH84001 and the 180 My old martian meteorite EETA79001 as compared to measurements made of the current martian atmosphere by the Viking spacecraft in 1976.

a second high temperature plateau of different age in the many different age spectra that have been measured [33, 83, 101]. However, note that if the subpopulation of 4.4 Ga laser probe dates is not an artifact but instead is reflective of isolated locations in ALH84001 that escaped late heating [83], the D3 event may not have completely reset the $^{40}Ar/^{39}Ar$ chronometer everywhere in the meteorite.

That even one of the two dozen known martian meteorites has been this cool for so long gives evidence of great differences in the extent and duration of igneous and tectonic processes on Earth and Mars. Perhaps even more remarkably, using a linear extrapolation of the Arrhenius relationship down to low temperatures, we find that ALH84001 could not have been held at a constant temperature

exceeding -70◦C ± 4◦C during the last 4 Gyr prior to its ejection from Mars (otherwise, it would have lost more than 5% of its ^{40}Ar). Any temperature excursions during the last 4 Gyr to 0◦C as short-lived as ~10^4 to 10^5 yr are also contradicted. It is important to note that the quoted uncertainty 4◦C is estimated from the formal errors in the Arrhenius relationship yielded by the regression analysis, and does not include the very large uncertainty resulting from the possibility that our bold extrapolation of *D* (through six orders of magnitude) is inappropriate. In particular, had we used our alternate (but less favored) Arrhenius relationship derived from the low temperature release data (see Section 2), the limiting temperature becomes -25◦C.

Interestingly, this limiting -70◦C temperature is near the center of the present-day range of average surface temperatures (~ -90◦C to -40◦C) in martian mid- to high latitudes. The likelihood that Mars' obliquity (and surface temperatures) have periodically reached high values [119] can be reconciled with these constraints if during the last 4 Ga, ALH84001 was buried at depths > ~0.1 to 1 km (depending on its latitude and the frequency of the obliquity oscillations), where it would be shielded from the obliquity-induced, seasonal, and diurnal thermal waves. In summary, if our extrapolation of the diffusion coefficient is not grossly inaccurate, this suggests that for most of the last 4 Gyr, average temperatures near the martian surface may not have been significantly warmer than those today. Future studies of ALH84001 using thermochronometers with closure temperatures lower than that of ^{40}Ar/^{39}Ar (e.g., (U-Th)/He) could rigorously test this possibility.

Epilogue

SOME SPECULATIONS ON MARS, PANSPERMIA, AND THE ORIGIN OF LIFE

During the nineteenth century, when steady state cosmological theories were in vogue, Lord Kelvin, Svante Arrhenius, and other eminent scientists believed that the transfer of life from one planet to another was a process made inevitable by the infinite extent and duration of the universe. This hypothesis, known as panspermia, subsequently fell out of favor, partly as a result of the acceptance of the Big Bang theory. Most efforts to understand the origin of life have since been framed by the assumption that life began on Earth.

However, in the last decade data have begun to accumulate suggesting that panspermia may in fact be a natural and frequently occurring process. Recent paleomagnetic studies on martian meteorite ALH84001 (Chapters 2 and 4) suggest that this rock traveled from Mars to Earth without its interior becoming warmer than 40ºC [5] (Fig. 5.1). Experiments aboard the European Space Agency's Long Duration Exposure Facility indicate that bacterial spores can survive in deep space for more than five years [36, 120], and laboratory experiments demonstrate that bacteria can survive the shocks and jerks expected for a rock ejected from Mars [121]. Finally, dynamical studies indicate that the transfer of rocks from Mars to Earth (and to a limited extent, *vice versa*) can proceed on a biologically short time scale, making it likely that organic hitchhikers have traveled between these planets many times during the history of the Solar System [122, 123]. These studies demand a re-evaluation of the long-held assumption that terrestrial life evolved in isolation on Earth.

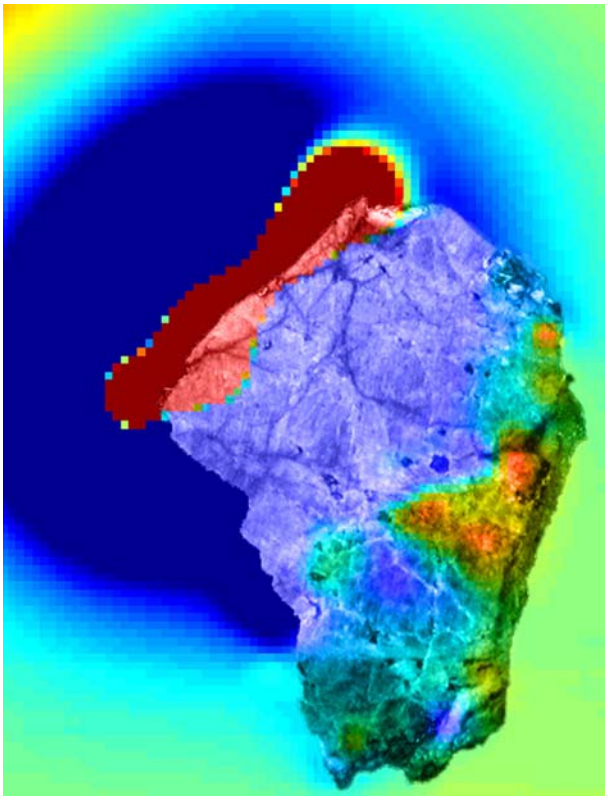

Fig 5.1 Magnetic scan of a slice of ALH84001,228b superimposed on its optical image. Intensity of the perpendicular component of the magnetic field is depicted with a red and blue color scale (corresponding to field lines oriented out-of-the-page and into-the-page, respectively). Note the large magnetic anomaly centered on the fusion crust, and the baked zone that extends less than a few mm inwards from it. The center of the rock has a heterogeneous magnetic pattern, indicating that it probably has not been heated even to ~40ºC since before 15 Ma [5]. This implies that rocks can travel between Mars and Earth without being heat sterilized.

Three lines of evidence have been proposed to support the idea that by 4.0 billion years ago (Ga), life somewhere had evolved to a fairly high level of complexity. These challenge the assumption that the late heavy bombardment [102] was inimical to the origin and continuity of life. First, the presence of isotopically depleted graphite inclusions in apatite crystals in Archean rocks from Greenland [124] were interpreted as the action of biological carbon fractionation, perhaps through photosynthesis. However, this has been cast in doubt because the apatite has U/Pb and Pb/Pb ages of ~1.5 Ga, indicating either that they formed

much later than the BIFs and/or their isotopic ratios were reset by a high-temperature metamorphic event [125]. The geological context of the sampling area has also been questioned [126].

The second line of evidence is the possible presence of 3.9 to 4.1 Ga magnetofossils (indistinguishable from those made by modern Earthly bacteria) in the ALH84001 carbonates [19, 127, 128]. Although this hypothesis remains highly controversial, no one has yet documented a plausible, inorganic mechanism for producing similar particles. The ferrite industry (which makes small magnetic particles for disk drives and magnetic recording tapes, and is worth $35 billion per year) has tried to make similar particles of magnetite inorganically for the past 60 years and has failed. The inorganic synthesis of magnetosome-like magnetite particles is clearly not a simple feat. Although Golden *et al.* [129] claim to have produced magnetofossil-like magnetites from heating of siderite, they have not yet documented the shape and chemistry of those inorganic magnetites in detail (see [128]). Nevertheless, their mechanism should be studied further given that shocks have probably affected ALH84001 carbonates.

The third line of evidence is recent molecular clock analyses which exploit the large number of completely sequenced genomes of Bacteria, Archaea, and Eukarya, and indicate that the Last Common Ancestor (LCA) of all living organisms dates back to about 4 Ga [130] (Fig. 5.2). This phylogeny [130] is more pleasing than earlier attempts using fewer gene systems because it intrinsically agrees with two deep-time aspects of the direct geological record: it agrees with the presence of the first biomarkers (2-methylhopanoids) possibly indicative of the cyanobacteria at around 2.5 Ga [131], and with the direct fossil record of organelle-bearing eukaryotes at about 2.1 Ga [132]. Hence, it is

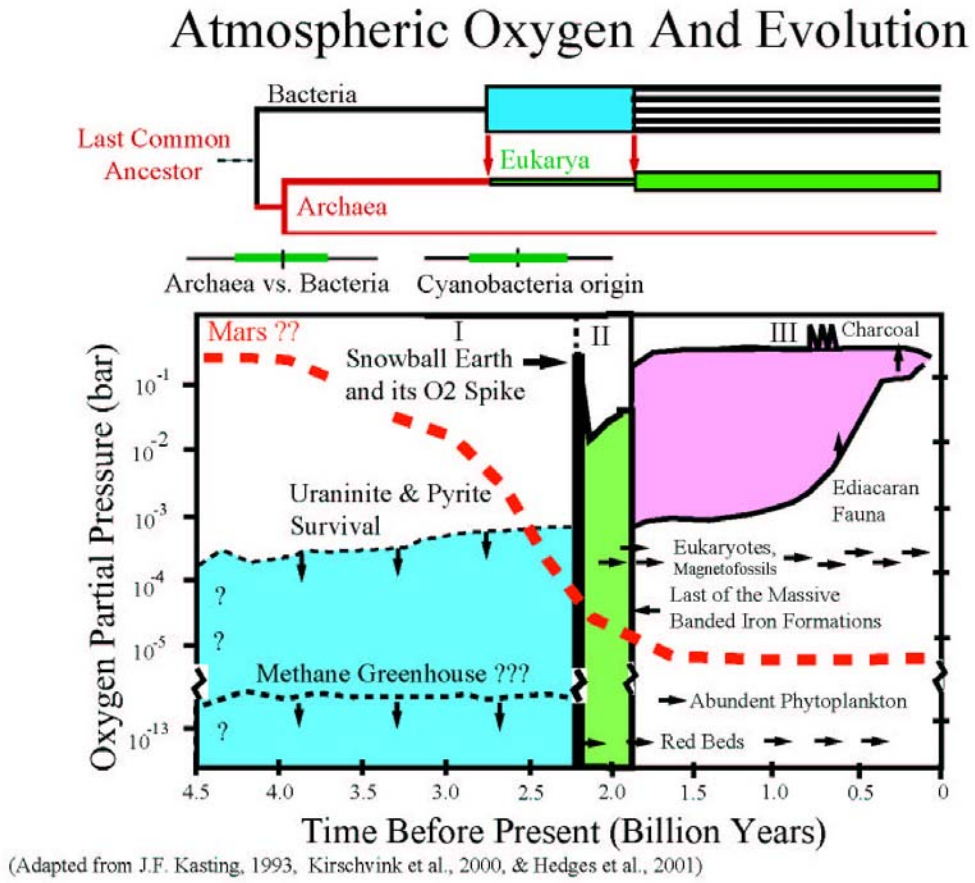

Fig. 5.2 Evolution of life compared to Earth and Mars. Biological evolution is compared with a schematic representation of the atmospheric partial pressures of oxygen in the Earth and martian atmospheres, as a function of geological time (horizontal axis). The horizontal lines along the top of the figure show the molecular clock estimates for the divergence times between the Bacteria, Archaea, and Eukaryotic Domains as recently estimated by Hedges *et al.* [130], with the position of the Last Common Ancestor (LCA) of all life shown in the upper left. Error bars slightly below this labeled "Archaea vs. Bacteria" show the 1 and 2σ error estimates for this LCA, and to the right of this similar errors are shown for the origin of the cyanobacteria (from [130]). Note that the cyanobacteria (and hence the O_2-releasing complex of Photosystem-II) evolved significantly later than the LCA. Colored horizontal bars below this show the geological distribution of rocks and fossil types which have implications for the oxygen concentrations in the atmosphere and shallow waters of the oceans, including the Banded Iron Formations (BIFs), red beds, magnetofossils and eukaryotes (same distribution), phytoplankton, animals, and charcoal (adapted loosely from [133]). The blue bar on the left of this shows the probable time interval during which the martian magnetic dynamo was active, shielding its atmosphere from erosion by the solar wind (partly constrained by the age of magnetization in ALH84001 [7]). The box in the lower part of the diagram shows the perceived history of atmospheric oxygen for Earth and Mars. For Earth, the light blue field between 4.5 and 2.3 Ga reflects the presence of detrital, stream-rounded pyrite and uraninite, reducing paleosols, BIFs, and Mn^{+2} incorporated into shallow-water carbonates, etc. The lower, deep-blue field shows the upper limit of 10^{-8} bar O_2 (estimated by [134]) for a methane-dominated greenhouse atmosphere, which may have been promoted by more reducing source regions for volcanic gasses in Earth's mantle during the first half of planetary history [135]. The vertical black bar at about 2.3 Ga shows

the ~70 Ma duration of the Paleoproterozoic Snowball Earth and the associated Kalahari Manganese Field which was deposited in its aftermath [136]; presumably as a result of the evolution of Photosystem-II in pre-existing cyanobacteria), with the resultant massive release of O_2 and the collapse of the methane greenhouse [134]. Following this, the green field shows the transition from the post-Snowball episode until the depletion of ferrous iron at all levels of the world oceans (and an end to this buffering). The pink field indicates the subsequent rise in O_2 level to modern values, including 3 ± 1 spikes in O_2 anticipated from cyanobacterial blooms following the Neoproterozoic Snowball events [136]. The red dotted line for Mars is anchored by the current atmospheric concentration of O_2, and is speculatively extended back in time for the inferred thicker atmosphere earlier in its history. We show it as a peak at 4.0 Ga to reflect the possible presence of ozone in the martian atmosphere inferred from mass-independent fractionation of oxygen in ALH84001 carbonates [137], and infer a positive slope before this as a result of magnetic shielding of the martian atmosphere by a geodynamo during which H (but not O) was lost to space.

probably the Hadean of Earth, or perhaps even the Noachian of Mars, in which we must look for Darwin's "warm little pond".

Because life on Earth depends on a variety of biochemical respiratory chains involving electron transport, we argue that the presence of electrochemical gradients is one of the most critical prerequisites for life's initiation and would form intense selection pressures during its initial evolution. A recent genetic analysis of the respiratory chains in the Archaea, Eukarya and Bacteria [138] indicates that terminal oxidases linked to oxygen, nitrate, sulfate, and sulfur were all present in the last common ancestor of living organisms. An alternative interpretation, massive lateral gene transfer [139], can be ruled out at least for O_2 because most of the cytochrome oxidase genes (with the exception of a small domain in one organism) track the phylogeny of rRNA [140]. Figure 5.3 shows the typical electrochemical cascades that operate in a modern, neutral oceanic system, with the basal oxidase of the LCA indicated in red. Our LCA must have evolved on a world in which these redox gradients were present in large enough quantities to evolve and to be maintained, and in which metastable, energetic compounds could diffuse across redox boundaries. "Smothered" environments (like Europa's ocean [141]) that lack significant electrochemical gradients are difficult for existing life to survive in, and would have been even more difficult for it to arise in. Since the efficiency of biological systems tends to improve over

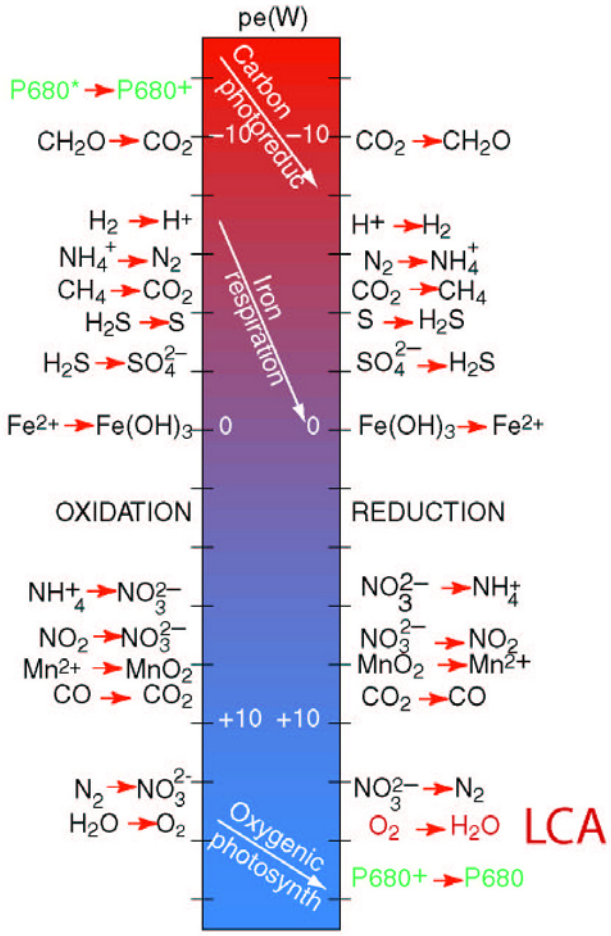

Fig. 5.3 Typical redox couples in neutral seawater (adapted from [141]). Half-reactions on the left couple spontaneously with those below them on the right. The red couple on the lower right indicates the lowest redox level (down to molecular O_2) achieved by respiratory chains in the Last Common Ancestor [138] prior to about 4 Ga [130].

time as a result of the processes of random mutation and natural selection [142], primitive metabolic electron transport systems likely could not extract energy as efficiently from the redox couples shown in Figure 5.3 as do those of modern organisms. In fact, many of the intermediate steps in these electron transport chains arose through gene duplication events from ancestral proteins [140]. Hence, the ancestral forms could not have been as efficient at recovering metabolic energy as are the modern ones. For this reason, we argue that life is

more likely to have evolved on the planet (either Earth or Mars) that had the broadest dynamical range of electrochemical species early in its history.

So now it is important to compare the probable environments of the early Earth with that of early Mars in order to evaluate which of these two bodies, during the first half-billion years of the solar system, might have produced an environment most suitable for the origin of life based on redox chemistry. This involves deducing the early environments of Mars and of Earth during a time interval when Earth lacks an extensive sedimentary rock record and when the martian record must be accessed indirectly. Likewise, the principal gaseous components produced by volcanic emissions likely had equilibrated with the reducing components then present in the outer mantles of these planetary bodies. A recent study of martian meteorites [143] has shown that the mantle of Mars is more reduced than that of the Earth, while the crust of Mars is still quite oxidized. The difference between the two planets is probably a result of the fact that Mars lacks plate tectonics, which on Earth recycles oxidized crust back into the mantle, plate tectonics did not necessarily oxidize the mantle quickly. Kump *et al.* [135] argue that during Archean time subducted oceanic crust may well have penetrated to the lower mantle, implying that the bulk of volcanic gasses equilibrated with the more primitive and more reducing upper mantle, until a turn-over event near the Archean/Proterozoic boundary. Both planets, then, possessed at least local environments sufficiently reducing to allow the accumulation of pre-biotic compounds. The question then focuses on determining which planet would have contained a better source of oxidizing atmospheric compounds capable of diffusing into this primordial soup to promote organic evolution.

Figure 5.2 (adapted from [133]) shows the redox history of Earth's surface, as inferred through the geological record. Although today both Earth and Mars

have extremely oxidizing surficial environments, there has been a long debate about the redox potential of the Earth's surface prior to the Phanerozoic (summarized in [144]). Sedimentary rocks of Archean and early Proterozoic age typically contain banded iron formations (BIFs) and detrital, stream-rounded pebbles of the minerals pyrite and uraninite. Based on modern analogs, these are usually taken as indicative of more reducing conditions. In contrast, the strongest line of evidence for oxygen production in the Archean was the presence of filaments with strong similarities to cyanobacteria from black cherts in the 3.5 Ga Warawoona group of Australia [145, 146]. These claims supported an environmental model of small oxygenic "islands" of photosynthetic life separated by sharp redox gradients from an otherwise anaerobic environment (e.g., [147]). However, Buick [148] has maintained that the actual black cherts sampled for these studies were secondary hydrothermal silica deposits of much younger age which cross-cut the primary bedding (an observation with which we concur after having visited these localities with him this past July). These putative fossils are probably not a constraint on oxygen in the Archean environment. Furthermore, it is unclear why the cyanobacteria, if equipped with the incredible power of the oxygen-releasing Photosystem-II, did not follow an explosive exponential growth pattern to take over the world as soon as they evolved. Even the presence of Archean stromatolites does not help, given their possible abiogenicity [149] and the possibility that their photosystems were non-oxygenic. In fact, the oldest direct evidence for oxygenic photosynthesis (Photosystem-II) is the Kalahari Manganese Field, which precipitated as oxides in the aftermath of the Paleoproterozoic Snowball glaciation event at about 2.3 Ga [136]. These deposits could well be the result of run-away oxygenation of the surface environment as a result of the newly evolved Photosystem-II. As shown on Fig. 5.2, the Kalahari Manganese Field falls well within the error range for the evolution of cyanobacteria given by the

Hedges *et al.* [130] molecular-clock study, but it is clearly out of range for the LCA.

In recent years, several new developments have bolstered the case for a strongly reducing surficial environment on Earth during Archean and earliest Proterozoic time. First, shallow-water carbonates of this age typically contain a trace of Mn^{+2}, which is only soluble under anoxic conditions [136, 150], requiring oxidants of either nitrate or O_2 to be oxidized to the insoluble Mn^{+4} form (see Fig. 3). But nitrate formation in the ocean requires O_2 [136], so this is *de facto* a constraint on O_2. The Mn^{+2} presumably was incorporated in the carbonate during initial precipitation, but it disappears after the first Snowball event at 2.3 Ga. This implies that post-Snowball oxygen levels were high enough to keep Mn^{+2} out of solution in the surficial waters. Second, Sumner [151] has noted that Fe^{+2} has a strong inhibitory effect on the nucleation of carbonate minerals, and that many of the shallow-water early Archean carbonates display textures compatible with the presence of ferrous iron in the shallow, mixed surface waters.

Third, recent work on terrestrial mass-independent sulfur isotope fractionation [152] suggests that units older than the Snowball were derived from an environment reducing enough to allow gaseous sulfur compounds to be cycled within the atmosphere. The implications of sulfur fractionations for the early martian redox environment are less clear. Although ~4 Ga ALH84001 pyrites also show enormous mass-independent sulfur fractionations, these do not require a reducing atmosphere but instead can be explained by the lack of crustal recycling on Mars, in combination with an early influx of isotopically heterogeneous materials to the planet [153]. Furthermore, mass-independent fractionation of oxygen isotopes (^{17}O with reference to ^{16}O and ^{18}O) in

ALH84001 carbonates suggest passage of this element through an atmospheric ozone phase [137].

Fourth, the rarity of glacial features during Archean time, coupled with solar evolution models arguing for a faint-young-sun with 30% less luminosity than today, has long presented a climatic paradox in its own right. Suggestions of a massive, 10-bar CO_2 greenhouse atmosphere [133] conflict with lower estimates of atmospheric CO_2 from Archean paleosols [154]. However, Pavlov *et al.* [134] note that an Archean atmosphere rich in methane would solve this paradox, and would provide an elegant trigger for the Paleoproterozoic Snowball event as soon as Photosystem-II were to evolve. If these indicators are extrapolated blindly back to the Hadean Earth, environments capable of producing sharp redox gradients needed for the evolution of primitive life would be rare to nonexistent.

The temporal evolution of oxygen in the martian atmosphere is much less understood. In the present-day atmosphere, H and O atoms are thought to be lost from the atmosphere to space in a self-regulating ratio of 2:1, which maintains a constant oxidation state for the planet. This loss ratio is maintained today because the rates of formation and photolysis of H_2O adjust to maintain the appropriate supplies of free H and O available for loss [155]. The constant 2:1 loss ratio is maintained despite the fact that the principal loss mechanisms for these two elements are vastly different. Hydrogen is lost mainly via thermal escape [156]. On the other hand, O, a much heavier element, is lost chiefly from the impingement of the solar wind plasma and magnetic field (e.g., atmospheric sputtering, dissociative recombination, and direct ion pick-up [157, 158]). Both hydrogen and oxygen loss have had a much less significant effect on Earth's atmosphere both because of Earth's higher gravity and strong magnetic field (the latter reduces solar-wind-induced ionization as well as loss of ionized species due to interaction with the solar-wind magnetic field).

Although Mars currently lacks a global magnetic field, we have recently learned that it had a strong field at 4 Ga or earlier [45]. The ancient field would have protected against the loss of O [159]. If today's self-regulating loss mechanisms for H and O also operated in this early period in Mars history, this would imply that H loss would have also have been much less in this period. However, there are some reasons to believe that this was not the case. The D/H ratio of the present-day atmosphere is ~5 times that of the Earth, indicating that a large amount of H (and, by implication, H_2O) has been lost to space. However, the $^{18}O/^{16}O$ ratio is not much different than the terrestrial value, indicating that O and H loss were decoupled in the past [160]. This permits a scenario in which the protection afforded by the early magnetic field resulted in dramatically more loss of H than O and resulting in a cascade of oxidants to drive organic evolution. Given that Mars's mantle was conceivably more reduced than that of Earth [143], such oxidizing conditions at the surface would imply that Mars had much larger redox gradients than Earth at the same time.

Isotopic studies of the martian meteorite ALH84001 are consistent with a neutral to oxidizing surface environment in which the carbonates formed about 4 billion years ago, including contributions from photo-irradiated ozone [137]. This ozone would have shielded an early martian biosphere from UV radiation, a protection presumably lacking on Earth at the same time [161]. Also, the possible presence of magnetofossils in this meteorite argues for the presence of vertical redox gradients, which magnetotactic bacteria need for their survival [162]. The oldest magnetofossils yet identified on Earth are from the post-Snowball Gunflint Chert at about 2.1 Ga [162], roughly coincident with the appearance of the first eukaryotes [132]. At face value, all of these lines of evidence suggest that, compared to early Earth, early Mars might have had a greater supply of biologically useable energy and was perhaps, by implication, a better place for the

origin of life. And so we salute you, all you descendants of space-traveling microbes from the Red Planet!

GLOSSARY

For more details about rock magnetism and associated paleomagnetic techniques, see books by Dunlop and Özdemir [40] and Butler [38].

Domain: the region within a crystal in which electrons align together in a single direction as a result of quantum mechanical exchange interactions.

Single domain (SD) grain: a crystal that is small enough such that it only contains one domain, but large enough such that the exchange forces are sufficiently strong to stabilize the direction of this moment**.** SD grains are ideal for recording a magnetization that is stable through time. For magnetite, the SD size range is typically between 30 nm and 100 nm.

Superparamagnetic (SP) grain: a crystal that is too small to hold a directionally stable magnetization at some temperature for longer than a given time (usually 100 s at room temperature unless otherwise specified). Because they are not thermally stable, an assemblage of SP grains will not accurately record the direction or intensity of paleofields. For magnetite, the SP size range is typically below 30 nm.

Multidomain (MD) grain: a crystal that is so large that it contains several magnetic domains. Because these domains are unstable and are magnetized in many different directions, MD grains will not accurately record the direction or intensity of magnetic fields which magnetize them. For magnetite, the MD size range is typically above 10 μm.

Pseudo single domain (PSD) grain: a crystal sized between SD and MD and exhibiting intermediate behavior. For magnetite, the PSD size range is typically between 1 and 10 μm.

Natural remanent magnetism (NRM): the magnetization that is observed in a ferromagnetic material prior to laboratory treatment. NRM typically takes the form of

thermoremanent magnetism, crystallization remanent magnetism, or detrital remanent magnetism.

Thermoremanent magnetism (TRM): the magnetization produced in a ferromagnet when it cools below its blocking temperature in the presence of a magnetic field. TRM produced in SD grains in the Earth's field is typically an order of magnitude more intense than detrital and crystallization remanent magnetizations produced in the same field.

Detrital remanent magnetism (DRM): the magnetization produced in a sedimentary rock as a result of the settling and alignment of ferromagnetic crystals in the fluid during sediment deposition in the presence of a field. DRM is typically found in unaltered and unweathered rocks like shales, carbonates and sandstones.

Crystallization remanent magnetism (CRM): the magnetization produced in a ferromagnet when it first crystallizes in the presence of a magnetic field (usually at a low and constant temperature). CRM is typically found in low-temperature aqueous precipitates and alteration products (e.g., weathered rocks containing hematite or maghemite rust).

Shock remanent magnetism (SRM): A poorly understood magnetization that is apparently produced in some ferromagnets after exposure to shock in the presence of a field. SRM has never conclusively identified in natural rocks. It is not clear whether SRM results from the pressure or temperature rise during the passage of the shock wave. Laboratory experiments have showed that basalts shocked to moderate pressures (0.1 to 20 GPa) will in fact partly remagnetize (if a field is present) or partly demagnetize (if a field is absent).

Isothermal remanent magnetization (IRM): a magnetization that is acquired during short exposure to strong magnetic fields at constant temperature (e.g., by a lightning strike or in the lab from an artificial magnet). By determining the IRM field intensity required to saturate a rock's magnetization, one can infer the mineralogy of the ferromagnetic material in the rock (for example, magnetite typically saturates at 300 mT, but pyrrhotite saturates at 1000 mT).

Anhysteretic remanent magnetism (ARM): an artificial magnetization acquired during exposure to an alternating field (of slowly decaying amplitude) superimposed on a constant bias field.

Viscous remanent magnetism (VRM): a magnetization accumulated during long exposures to ambient magnetic fields at constant temperature. Rocks that contain a primary (e.g., thermo-) remanence typically acquire a small, younger VRM overprint that mostly affects the MD and the smallest SD grains. This occurs because remagnetization is ultimately a time- as well as temperature-dependant process.

Alternating field (AF) demagnetization: an artificial way of demagnetizing a rock by exposing it to an alternating field whose amplitude slowly decays to zero. By comparing progressive AF demagnetization of a rock that has been given an IRM to the AF demagnetization of the same rock given an ARM, one can infer the mean size and domain state (e.g., SD, PSD or MD) of the assemblage of ferromagnetic crystals in the rock.

Coercivity: The field intensity required to remagnetize a ferromagnetic crystal at room temperature. SP and MD crystals have much lower coercivities than SD grains (in fact, by definition, the coercivity of SP grains is 0). The larger an SD grain, the higher is its coercivity.

Blocking temperature: the temperature at which a single domain crystal is able to hold a directionally stable magnetization. The blocking temperature therefore is the temperature at which a grain goes from SD to SP (for a given heating time, typically 100 s). The larger the grain, the higher is its blocking temperature. The blocking temperature of the largest SD grains is the Curie point. Since rocks are typically composed of a suite of billions of ferromagnetic crystals of many different sizes, rocks will usually have crystals with blocking temperatures ranging continuously from the Curie point down to 0 K. Since remagnetization is actually a temperature *and time dependant* process, the blocking temperature concept is only a convenient approximation of the thermal stability of ferromagnets. In particular, the smallest SD grains will have different blocking temperatures for different times of exposure to those temperatures.

Curie point: the highest possible blocking temperature for a given ferromagnetic material. The Curie points of magnetite and pyrrhotite are 580ºC and 320ºC, respectively.

BIBLIOGRAPHY

[1] J.L. Kirschvink, How sensitive should a rock magnetometer be for use in paleomagnetism?, in: SQUID Applications to Geophysics., H. Weinstock and W.C. Overton, eds., pp. 111-114, The Society of Exploration Geophysicists, Tulsa, Oklahoma, 1981.

[2] F.J. Baudenbacher, N.T. Peters and J.P. Wikswo, High resolution low-temperature superconductivity superconducting quantum interference device microscope for imaging magnetic fields of samples at room temperatures, Rev. Sci. Instrum. 73 (2002) 1247-1254.

[3] J.P. Wikswo Jr., High-resolution magnetic imaging: Cellular action currents and other applications, in: SQUID Sensors: Fundamentals, Fabrication and Applications, H. Weinstock, ed., pp. 307-360, Kluwer Academic Publishers, The Netherlands, 1996.

[4] J.R. Kirtley and J.P. Wikswo, Scanning SQUID Microscopy, Ann. Rev. Mater. Sci. 29 (1999) 117-148.

[5] B.P. Weiss, J.L. Kirschvink, F.J. Baudenbacher, H. Vali, N.T. Peters, F.A. MacDonald and J.P. Wikswo, A low temperature transfer of ALH84001 from Mars to Earth, Science 290 (2000) 791-795.

[6] B.P. Weiss, F.J. Baudenbacher, J.P. Wikswo and J.L. Kirschvink, Magnetic microscopy promises a leap in sensitivity and resolution, Eos Trans. AGU 82 (2001) 513 & 518.

[7] B.P. Weiss, H. Vali, F.J. Baudenbacher, J.L. Kirschvink, S.T. Stewart and D.L. Shuster, Records of an ancient Martian magnetic field in ALH84001, Earth Planet. Sci. Lett. 201 (2002) 449-463.

[8] H.J. Melosh, The rocky road to panspermia, Nature 332 (1988) 687-688.

[9] H.J. Melosh, Meteorite origins - Blasting rocks off planets, Nature 363 (1993) 498-499.

[10] A.J. Gratz, W.J. Nellis and N.A. Hinsey, Observations of high-velocity, weakly shocked ejecta from experimental impacts, Nature 363 (1993) 522-524.

[11] V.A. Bronshten, Physics of Meteoric Phenomena, 52-56 pp., Kluwer Academic, Boston, 1983.

[12] L.E. Nyquist, B. Bansal, H. Wiesmann and C.-Y. Shih, "Martians" young and old: Zagami and ALH84001, Lunar Planet. Sci. XXVI (1995) 1065-1066.

[13] D. McKay, E. Gibson, K. Thomas-Keprta, H. Vali, C. Romanek, S. Clemett, X. Chillier, C. Maechling and R. Zare, Search for past life on Mars - Possible relic biogenic activity in Martian Meteorite ALH84001, Science 273 (1996) 924-930.

[14] L.E. Borg, J.N. Connelly, L.E. Nyquist, C.Y. Shih, H. Wiesmann and Y. Reese, The age of the carbonates in martian meteorite ALH84001, Science 286 (1999) 90-94.

[15] A.H. Treiman, The history of Allan Hills 84001 revised: Multiple shock events, Meteorit. Planet. Sci. 33 (1998) 753-764.

[16] T.D. Swindle, J.A. Grier and M.K. Burkland, Noble gases in orthopyroxenite ALH84001 - A different kind of Martian meteorite with an atmospheric signature, Geochim. Cosmochim. Acta 59 (1995) 793-801.

[17] B.J. Gladman, J.A. Burns, M. Duncan, P. Lee and H.F. Levison, The exchange of impact ejecta between terrestrial planets, Science 271 (1996) 1387-1392.

[18] J.L. Kirschvink, A.T. Maine and H. Vali, Paleomagnetic evidence of a low-temperature origin of carbonate in the Martian meteorite ALH84001, Science 275 (1997) 1629-1633.
[19] K.L. Thomas-Keprta, D.A. Bazylinski, J.L. Kirschvink, S.J. Clemett, D.S. McKay, S.J. Wentworth, H. Vali, E.K. Gibson Jr. and C.S. Romanek, Elongated prismatic magnetite crystals in ALH84001 carbonate globules: Potential Martian magnetofossils, Geochim. Cosmochim. Acta 64 (2000) 4049-4081.
[20] D.W. Collinson, Magnetic properties of Martian meteorites - Implications for an ancient Martian magnetic field, Meteorit. Planet. Sci. 32 (1997) 803-811.
[21] S.M. Cisowski and M. Fuller, The effect of shock on the magnetism of terrestrial rocks, J. Geophys. Res. 83 (1978) 3441-3458.
[22] I.M. Thomas, T.C. Moyer and J.P. Wikswo, High resolution magnetic susceptibility imaging of geological thin sections: pilot study of a pyroclastic sample from the Bishop Tuff, Geophys. Res. Lett. 19 (1992) 2139-2142.
[23] C.K. Shearer, L.A. Leshin and C.T. Adcock, Olivine in Martian meteorite Allan Hills 84001: Evidence for a high-temperature origin and implications for signs of life, Meteorit. Planet. Sci. 34 (1999) 331-339.
[24] A.J. Brearley, Hydrous phases in ALH84001: Further evidence for preterrestrial alteration and shock-induced thermal overprint, Lunar Plan. Sci. XXXI (2000) Abstract #1203.
[25] B. Gladman, Destination: Earth. Martian meteorite delivery, Icarus 130 (1997) 228-246.
[26] J.N. Goswami, N. Sinha, S.V.S. Murty, R.K. Mohapatra and C.J. Clement, Nuclear tracks and light noble gases in Allan Hills 84001: Preatmospheric size, fall characteristics, cosmic-ray exposure duration and formation age, Meteorit. Planet. Sci. 32 (1997) 91-96.
[27] J.L. Bada, G. D.P., M. G.D. and B. L., A search for endogenous amino acids in martian meteorite ALH84001, Science 279 (1998) 362-365.
[28] N. Sugiura and H. Hoshino, Hydrogen-isotopic compositions in Allan Hills 84001 and the evolution of the martian atmosphere, Meteorit. Planet. Sci. 35 (2000) 373-380.
[29] A. Menyeh and W. O'Reilly, Thermoremanent magnetization in monodomain monoclinic pyrrhotite Fe_7S_8, J. Geophys. Res. 101 (1996) 25045-25051.
[30] D.J. Dunlop, O. Ozdemir, D.A. Clark and P.W. Schmidt, Time-temperature relations for the remagnetization of pyrrhotite (Fe_7S_8) and their use in estimating paleotemperatures, Earth Planet. Sci. Lett. 176 (2000) 107-116.
[31] G. Pullaiah, G. Irving, K.L. Buchan and D.J. Dunlop, Magnetization changes caused by burial and uplift, Earth Planet. Sci. Lett. 28 (1975) 133-143.
[32] H.J. Melosh, Impact Cratering: A Geologic Process, 245 pp., Oxford University Press, Oxford, 1986.
[33] D.D. Bogard and D.H. Garrison, Argon-39-argon-40 "ages" and trapped argon in Martian shergottites, Chassigny, and Allan Hills 84001, Meteorit. Planet. Sci. 34 (1999) 451-473.
[34] J.D. Gilmour, J.A. Whitby and G. Turner, Xenon isotopes in irradiated ALH84001: Evidence for shock-induced trapping of ancient Martian atmosphere, Geochim. Cosmochim. Acta 62 (1998) 2555-2571.

[35] B.J. Gladman and J.A. Burns, Mars meteorite transfer: Simulation, Science 274 (1996) 161-162.
[36] G. Horneck, H. Bucker and G. Reitz, Long-term survival of bacterial-spores in space, Adv. Space Res. 14 (1994) 41-45.
[37] B.E. Digregorio, G.V. Levin and P.A. Straat, Mars: The Living Planet, Frog Ltd., 1997.
[38] R.F. Butler, Paleomagnetism: magnetic domains to geologic terranes, 319 pp., Blackwell Scientific Publications, Boston, 1992.
[39] A. Menyeh and W. O' Reilly, The coercive force of fin particles of monoclinic pyrrhotite (Fe_7S_8) studied at elevated temperature, Phys. Earth Planet. Int. 89 (1995) 51-62.
[40] D.J. Dunlop and O. Ozdemir, Rock Magnetism: Fundamentals and Frontiers, 573 pp., Cambridge University Press, New York, 1997.
[41] M. Fuller and S.M. Cisowski, Lunar paleomagnetism, in: Geomagnetism, J.A. Jacobs, ed. 2, pp. 307-455, Academic Press, Orlando, 1987.
[42] K. Zapletal, Self-reversal of isothermal remanent magnetization in a pyrrhotite (Fe_7S_8) crystal, Phys. Earth Planet Inter. 70 (1992) 302-311.
[43] M. Bina and L. Daly, Minerological change and self-reversed magnetizations in pyrrhotite resulting from partial oxidation; geophysical implications, Phys. Earth Planet. Inter. 85 (1994) 83-89.
[44] A.H. Treiman, Heterogeneity of remanent magnetism in ALH84001: petrologic constraints, Lunar Planet. Sci. XXXI (2000) abstract #1225.
[45] M. Acuna, J. Connerney, N. Ness, R. Lin, D. Mitchell, C. Carlson, J. McFadden, K. Anderson, H. Reme, C. Mazelle, D. Vignes, P. Wasilewski and P. Cloutier, Global distribution of crustal magnetization discovered by the Mars Global Surveyor MAG/ER experiment, Science 284 (1999) 790-793.
[46] G. Schubert, C.T. Russell and W.B. Moore, Timing of the Martian dynamo, Nature 408 (2000) 666-667.
[47] D.W. Collinson, Magnetic properties of Antarctic shergottite meteorites EETA79001 and ALHA77005: Possible relevance to a Martian magnetic field, Earth Planet. Sci. Lett. 7 (1986) 159-164.
[48] S.M. Cisowski, Magnetism of meteorites, in: Geomagnetism, J.A. Jacobs, ed. 2, pp. 525-560, Academic Press, London, 1987.
[49] S.M. Cisowski, Magnetic studies on Shergotty and other SNC meteorites., Geochim. Cosmochim. Acta 50 (1986) 1043-1048.
[50] T. Nagata, Paleomagnetism of Antarctic achondrites, Mem. Natl. Inst. Polar Res. Spec. Issue 17 (1980) 233-242.
[51] P. Rochette, J.P. Lorand, G. Fillion and V. Sautter, Pyrrhotite and the remanent magnetization of SNC meteorites: a changing perspective on Martian magnetism, Earth Planet. Sci. Lett. 190 (2001) 1-12.
[52] J. Shaw, M.J. Hill and S.J. Openshaw, Investigating the ancient Martian magnetic field using microwaves, Earth Planet. Sci. Lett. 190 (2001) 103-109.
[53] M. Wadhwa, S.R. Sutton, G.J. Flynn and M. Newville, Microdistributions of Rb and Sr in ALH84001 carbonates: Chronological implications for secondary alteration on Mars, Lunar Planet. Sci. XXXIII (2002) abstract #1362.
[54] B.P. Weiss, H. Vali, S.T. Stewart and J.L. Kirschvink, Records of an ancient Martian magnetic field in ALH84001, Lunar Planet. Sci. XXXII (2001) abstract #1244.

[55] J.P. Greenwood and H.Y. McSween, Petrogenesis of Allan Hills 84001: Constraints from impact-melted feldspathic and silica glasses, Meteorit. Planet. Sci. 36 (2001) 43-61.

[56] R. Egli and F. Heller, High-resolution imaging using a high-Tc superconducting quantum interference device (SQUID) magnetometer, J. Geophys. Res. 105 (2000) 25709-25727.

[57] N.R. Nowaczyk, H.-U. Worm, A. Knecht. and J.H. Hinken, Imaging distribution patterns of magnetic minerals by a novel high-Tc-SQUID-based field distribution measuring system: Applications to Permian sediments, Geophys. J. Int. 132 (1998) 721-726.

[58] H. Sakai, K. Shirai, M. Takani, M. Horii and M. Funaki, Analysis of fine structure of chert and BIF by measurement of high resolution magnetic field and scanning x-ray analyzed microscope, Proc. NIPR Symp. Antarc. Geosci. 10 (1997) 59-67.

[59] A.P. Taylor, Magnetotactic Bacteria and Their Biominerals, Ph.D. Thesis, The University of Queensland, 2001.

[60] R.F. Butler and S.K. Banerjee, Theoretical single-domain size range in magnetite and titanomagnetite, J. Geophys. Res. 80 (1975) 4049-4058.

[61] J.C. Diaz Ricci and J.L. Kirschvink, Magnetic domain state and coercivity predictions for biogenic greigite (Fe_3S_4): A comparison of theory with magnetosome observations, J. Geophys. Res. 97 (1992) 17309-17315.

[62] R.S. Coe, S. Grommé and E.A. Mankinen, Geomagnetic paleointensities from radiocarbon-dated lava flows on Hawaii and the question of the Pacific nondipole low, J. Geophys. Res. 83 (1978) 1740-1756.

[63] R.S. Coe, The effect of magnetic interactions on paleointensity determination by the Thellier's method, J. Geomag. Geolectr. 26 (1974) 311-317.

[64] J.M. Eiler, J.W. Valley, C.M. Graham and J. Fournelle, Two populations of carbonate in ALH84001: Geochemical evidence for discrimination and genesis, Geochim. Cosmochim. Acta 66 (2002) 1285-1303.

[65] R.A. Langel and W.J. Hinze, The Magnetic Field of the Earth's Lithosphere, 429 pp., Cambridge University Press, Cambridge, 1998.

[66] M.E. Purucker, T.J. Sabaka and R.A. Langel, Conjugate gradient analysis: a new tool for studying satellite magnetic data sets, Geophys. Res. Lett. 23 (1996) 507-510.

[67] W.H. Press, S.A. Teukolsky, W.T. Vetterling and B.P. Flannery, Numerical Recipes in Fortran 77: The Art of Scientific Computing, 933 pp., Cambridge University Press, Cambridge, 1992.

[68] D.W. Mittlefehldt, ALH84001, a cumulate orthopyroxenite member of the Martian meteorite clan, Meteoritics 29 (1994) 214-221.

[69] A. Kumar and M.S. Bhalla, A source of stable remanence in chromite ores, Geophys. Res. Lett. 11 (1984) 177-180.

[70] Y.J. Yu, D.J. Dunlop, O. Ozdemir and H. Ueno, Magnetic properties of Kurokami pumices from Mt. Sakurajima, Japan, Earth Planet. Sci. Lett. 192 (2001) 439-446.

[71] J.W. Valley, J.M. Eiler, C.M. Graham, E.K. Gibson, C.S. Romanek and E.M. Stolper, Low-temperature carbonate concretions in the Martian meteorite ALH84001: Evidence from stable isotopes and mineralogy, Science 275 (1997) 1633-1638.

[72] H.Y. McSween and R.P. Harvey, An evaporation model for formation of carbonates in the ALH84001 Martian meteorite, Int. Geol. Rev. 40 (1998) 774-783.

[73] E.R.D. Scott, A.N. Krot and A. Yamaguchi, Carbonates in fractures of Martian meteorite Allan Hills 84001: Petrologic evidence for impact origin, Meteorit. Planet. Sci. 33 (1998) 709-719.
[74] J.P. Bradley, H.Y. McSween and R.P. Harvey, Epitaxial growth of nanophase magnetite in Martian meteorite, Meteorit. Planet. Sci. 33 (1998) 765-773.
[75] A. Schult, Effect of pressure on the Curie temperature of titanomagnetites [(1-x)Fe_3O_4 - $x$$TiFe_2O_4$], Earth Planet. Sci. Lett. 10 (1970) 81-86.
[76] T. Cooney, E. Scott, A. Krot, S. Sharma and A. Yamaguchi, Vibrational spectroscopic study of minerals in the Martian meteorite ALH84001, Am. Mineral. 84 (1999) 1569-1576.
[77] A. Bischoff and D. Stoffler, Shock metamorphism as a fundamental process in the evolution of planetary bodies: Information from meteorites, Eur. J. Mineral. 4 (1992) 707-755.
[78] T. Sekine, T.S. Duffy, A.M. Rubin, W.W. Anderson and T.J. Ahrens, Shock compression and isentropic release of granite, Geophys. J. Int. 120 (1995) 247-261.
[79] A.J.R. Kent, I.D. Hutcheon, F.J. Ryerson and D.L. Phinney, The temperature of formation of carbonate in Martian meteorite ALH84001: Constraints from cation diffusion, Geochim. Cosmochim. Acta 65 (2001) 311-321.
[80] D.A. Kring, T.D. Swindle, J.D. Gleason and J.A. Grier, Formation and relative ages of maskelynite and carbonate in ALH84001, Geochim. Cosmochim. Acta 62 (1998) 2155-2166.
[81] M.R. Baer, Computational modeling of heterogeneous reactive materials at the mesoscale, in: Eleventh Conference on Shock Compression of Condensed Matter, M.D. Furnish, L.C. Chhabildas and R.S. Hixson, eds. 1, pp. 27-33, American Institute of Physics, Snowbird, Utah, 1999.
[82] V. Malavergne, F. Guyot, K. Benzerara and I. Martinez, Description of new shock-induced phases in the Shergotty, Zagami, Nakhla and Chassigny meteorites, Meteorit. Planet. Sci. 36 (2001) 1297-1305.
[83] G. Turner, S.F. Knott, R.D. Ash and J.D. Gilmour, Ar-Ar chronology of the Martian meteorite ALH84001: Evidence for the timing of the early bombardment of Mars, Geochim. Cosmochim. Acta 61 (1997) 3835-3850.
[84] B.P. Weiss, D.L. Shuster and S.T. Stewart, Temperatures on Mars from $^{40}Ar/^{39}Ar$ thermochronology of ALH84001, Earth Planet. Sci. Lett. 201 (2002) 465-472.
[85] S.A. Gilder, M. LeGoff, J. Peyronneau and J.-C. Chervin, Novel high pressure magnetic measurements with application to magnetite, Geophys. Res. Lett. 29 (2002) 10.1029/2001GL014227.
[86] C.J. Hale, The intensity of the geomagnetic field at 3.5 Ga - Paleointensity results from the Komati Formation, Barberton Mountain Land, South Africa, Earth Planet. Sci. Lett. 86 (1987) 354-364.
[87] M. Hart and M. Fuller, Magnetization of a dolomite bed in the Monterey Formation: Implications for diagenesis, Geophys. Res. Lett. 15 (1988) 491-494.
[88] M. Fuller, S. Cisowski, M. Hart, R. Haston, E. Schmidke and R. Jarrard, NRM:IRM(s) demagnetization plots; an aid to the interpretation of natural remanent magnetization, Geophys. Res. Lett. 15 (1988) 518-521.
[89] D.A. Crawford and P.H. Schultz, Laboratory observations of impact-generated magnetic fields, Nature 336 (1988) 50-52.

[90] L.L. Hood and Z. Huang, Formation of magnetic-anomalies antipodal to lunar impact basins - 2-Dimensional model-calculations, J. Geophys. Res. 96 (1991) 9837-9846.
[91] D.W. Collinson, Magnetism of the Moon - A lunar core dynamo or impact magnetization?, Surv. Geophys. 14 (1993) 89-118.
[92] W.K. Hartmann and G. Neukum, Cratering chronology and the evolution of Mars, Space Sci. Rev. (2001) 165-194.
[93] D.J. Stevenson, T. Spohn and G. Schubert, Magnetism and thermal evolution of the terrestrial planets, Icarus 54 (1983) 466-489.
[94] G. Schubert and T. Spohn, Thermal history of Mars and the sulfur content of its core, J. Geophys. Res. 95 (1990) 14095-14104.
[95] F. Nimmo and D. Stevenson, Influence of early plate tectonics on the thermal evolution and magnetic field of Mars, J. Geophys. Res. 105 (2000) 11969-11979.
[96] D.J. Stevenson, Mars core and magnetism, Nature 412 (2001) 214-219.
[97] M.T. Zuber, The crust and mantle of Mars, Nature 412 (2001) 220-227.
[98] E. Jagoutz, A. Sorowka, J.D. Vogel and H. Wänke, ALH84001: Alien or progenitor of the SNC family?, Meteoritics 29 (1994) 478-479.
[99] A. Yamaguchi and T. Sekine, Monomineralic mobilization of plagioclase by shock: an experimental study, Earth Planet. Sci. Lett. 175 (2000) 289-296.
[100] Y.N. Miura, K. Nagao, N. Sugiura, H. Sagawa and K. Matsubara, Orthopyroxenite ALH84001 and shergottite ALHA77005: Additional evidence for a Martian origin from noble gases, Geochim. Cosmochim. Acta 59 (1995) 2105-2113.
[101] R.D. Ash, S.F. Knott and G. Turner, A 4-Gyr shock age for a martian meteorite and implications for the cratering history of Mars, Nature 380 (1996) 57-59.
[102] B.A. Cohen, T.D. Swindle and D.A. Kring, Support for the lunar cataclysm hypothesis from lunar impact melt ages, Science 290 (2000) 1754-1756.
[103] H. Fechtig and S.T. Kalbitzer, The diffusion of argon in potassium-bearing solids, in: Potassium Argon Dating, O.A. Schaeffer and J. Zahringer, eds., pp. 68-107, Springer-Verlag, New York, 1966.
[104] O. Eugster, H. Busemann and S. Lorenzetti, The pre-atmospheric size of Martian meteorites, Lunar Planet. Sci. XXXIII (2002) abstract #1096.
[105] H.S. Carslaw and J.C. Jaeger, The Conduction of Heat in Solids, 510 pp., Oxford University Press, London, 1959.
[106] M.H. Dodson, Closure temperature in cooling geochronological and petrological systems, Contr. Mineral. and Petrol. 40 (1973) 259-274.
[107] R.A. Wolf, K.A. Farley and D.M. Kass, Modeling of the temperature sensitivity of the apatite (U-Th)/He thermochronometer, Chem. Geol. 148 (1998) 105-114.
[108] I. McDougall and T.M. Harrison, Geochronology and Thermochronology by the $^{40}Ar/^{39}Ar$ Method, 269 pp., Oxford University Press, New York, 1999.
[109] C. Romano, J.E. Mungall, T. Sharp and D.B. Dingwell, Tensile strengths of hydrous vesicular glasses; an experimental study, Am. Mineral. 81 (1996) 1148-1154.
[110] J.C. Jaeger and N.G.W. Cook, Fundamentals of Rock Mechanics, 513 pp., Methuen and Co. Ltd., London, 1969.
[111] S.V.S. Murty and R.K. Mohapatra, Nitrogen and heavy noble gases in ALH 84001: Signatures of ancient Martian atmosphere, Geochim. Cosmochim. Acta 61 (1997) 5417-5428.

[112] M.M. Grady, I.P. Wright and C.T. Pillinger, A nitrogen and argon stable isotope study of Allan Hills 84001: Implications for the evolution of the Martian atmosphere, Meteorit. Planet. Sci. 33 (1998) 795-802.
[113] D.H. Garrison and D.D. Bogard, Isotopic composition of trapped and cosmogenic noble gases in several Martian meteorites, Meteorit. Planet. Sci. 33 (1998) 721-736.
[114] K. Marti and K.J. Mathew, Ancient Martian nitrogen, Geophys. Res. Lett. 27 (2000) 1463-1466.
[115] K.J. Mathew and K. Marti, Early evolution of Martian volatiles: Nitrogen and noble gas components in ALH84001 and Chassigny, J. Geophys. Res. 106 (2001) 1401-1422.
[116] D.D. Bogard, R.N. Clayton, K. Marti, T. Owen and G. Turner, Martian volatiles: Isotopic composition, origin, and evolution, Space Sci. Rev. 96 (2001) 425-458.
[117] K. Marti, J.S. Kim, A.N. Thakur, T.J. McCoy and K. Keil, Signatures of the martian atmosphere in glass of the Zagami meteorite, Science 267 (1995) 1981-1984.
[118] R.C. Wiens and R.O. Pepin, Laboratory shock emplacement of noble-gases, nitrogen, and carbon-dioxide into basalt, and implications for trapped gases in shergottite EETA-79001, Geochim. Cosmochim. Acta 52 (1988) 295-307.
[119] M. Carr, Water on Mars, 229 pp., Oxford University Press, Oxford, 1996.
[120] G. Horneck, European activities in exobiology in earth orbit: Results and perspectives, in: Life Sciences: Exobiology, Adv. Space Res. 23, pp. 381-386, 1999.
[121] R.M.E. Mastrapa, H. Glanzberg, J.N. Head, H.J. Melosh and W.L. Nicholson, Survival of bacteria exposed to extreme acceleration: implications for panspermia, Earth Planet. Sci. Lett. 189 (2001) 1-8.
[122] C. Mileikowsky, F.A. Cucinotta, J.W. Wilson, B. Gladman, G. Horneck, L. Lindegren, J. Melosh, H. Rickman, M. Valtonen and J.Q. Zheng, Natural transfer of viable microbes in space - 1. From Mars to Earth and Earth to Mars, Icarus 145 (2000) 391-427.
[123] B.P. Weiss and J.L. Kirschvink, Life from space? Testing panspermia with martian meteorite ALH84001, The Planetary Report 20 (2000) 8-11.
[124] S.J. Mojzsis, G. Arrhenius, K.D. Mckeegan, T.M. Harrison, A.P. Nutman and C.R.L. Friend, Evidence for life on Earth before 3,800 million years ago, Nature 384 (1996) 55-59.
[125] Y. Sano, K. Terada and Y.N. Takahashi, A. P., Origin of life from apatite dating?, Nature 400 (1999) 127.
[126] J.S. Myers and J.L. Crowley, Vestiges of life in the oldest Greenland rocks? A review of early Archean geology in the Godthabsfjord region, and reappraisal of field evidence for > 3850 Ma life on Akilia., Precambrian Research 103 (2000) 101-124.
[127] I.E. Friedmann, J. Wierzchos, C. Ascaso and M. Winklhofer, Chains of magnetite crystals in the meteorite ALH84001: Evidence of biological origin, Proc. Natl. Acad. Sci. USA 98 (2001) 2176-2181.
[128] K.L. Thomas-Keprta, S.J. Clemett, D.A. Bazylinski, J.L. Kirschvink, D.S. McKay, W. S.J., H. Vali, E.K.J. Gibson, M.F. McKay and C.S. Romanek, Truncated hexa-octahedral magnetite crystals in ALH84001: Presumptive biosignatures, Proc. Natl. Acad. Sci. USA 98 (2001) 2164-2169.
[129] D.C. Golden, D.W. Ming, C.S. Schwandt, H.V. Lauer, R.A. Socki, R.V. Morris, G.E. Lofgren and G.A. McKay, A simple inorganic process for formation of carbonates, magnetite, and sulfides in Martian meteorite ALH84001, Am. Mineral. 83 (2001) 370-375.

[130] S.B. Hedges, H. Chen, S. Kumar, D.Y.-C. Wang, A.S. Thompson and H. Watanabe, A genomic timescale for the origin of eukaryotes, BMC Evolutionary Biology 1:4 (2001).
[131] R.E. Summons, L.L. Jahnke, J.M. Hope and G.A. Logan, 2-methylhopanoids as biomarkers for cyanobacterial oxygenic photosynthesis, Nature 400 (2000) 554-557.
[132] T.M. Han and B. Runnegar, Megascopic eukaryotic algae from the 2.1 billion year old Negaunne iron-formation, Michigan, Science 257 (1992) 232-235.
[133] J.F. Kasting, Earth's early atmosphere, Science 259 (1993) 920-926.
[134] A.A. Pavlov, J.F. Kasting, L.L. Brown, K.A. Rages and R. Freedman, Greenhouse warming by CH_4 in the atmosphere of early Earth, J. Geophys. Res. 105 (2000) 11981-11990.
[135] L.R. Kump, J.F. Kasting and M.E. Barley, Rise of atmospheric oxygen and the "upside-down" archean mantle, Geochem. Geophys. Geosyst. 2 (2001) 2000GC000114.
[136] J.L. Kirschvink, E.J. Gaidos, L.E. Bertani, N.J. Beukes, J. Gutzmer, L.N. Maepa and R.E. Steinberger, Paleoproterozoic Snowball Earth: Extreme climatic and geochemical global change and its biological consequences., Proc. Natl. Acad. Sci. USA 97 (2000) 1400-1405.
[137] J. Farquhar, M.H. Thiemens and T. Jackson, Atmosphere-surface interactions on Mars: Delta O-17 measurements of carbonate from ALH 84001, Science 280 (1998) 1580-1582.
[138] J. Castresana and D. Moreira, Respiratory chains in the last common ancestor of living organisms, J. Mol. Evol. 49 (1999) 453-460.
[139] W.F. Doolittle, The nature of the universal ancestor and the evolution of the proteome, Curr. Opin. Struct. Biol. 10 (2000) 355-358.
[140] M. Schutz, M. Brugna, E. Lebrun, F. Baymann, R. Huber, K.O. Stetter, G. Hauska, R. Toci, D. Lemesle-Meunier, P. Tron, C. Schmidt and W. Nitschke, Early evolution of cytochrome bc complexes, J. Mol. Bio. 300 (2000) 663-675.
[141] E.J. Gaidos, K.H. Nealson and J.L. Kirschvink, Biogeochemistry - Life in ice-covered oceans, Science 284 (1999) 1631-1633.
[142] C. Darwin, On the origin of species by means of natural selection, or the preservation of favored races in the struggle for life, 502 pp., Cambridge University Press, Cambridge, 1859.
[143] M. Wadhwa, Redox state of Mars' upper mantle from Eu anomalies in Shergottite pyroxenes, Science 291 (2001) 1527-1530.
[144] J.W. Schopf and C. Klein, The Proterozoic Biosphere: A multidisciplinary Study, 1348 pp., Cambridge University Press, Cambridge, U.K., 1992.
[145] J.W. Schopf, Microfossils of the Early Archean Apex Chert - New evidence of the antiquity of life, Science 260 (1993) 640-646.
[146] J.W. Schopf and B.M. Packer, Early Archean (3.3-billion to 3.5-billion-year-old) microfossils from Warrawoona Group, Australia, Science 237 (1987) 70-73.
[147] P.E. Cloud, Oasis in space: Earth history from the beginning, 495 pp., W.W. Norton, New York, 1988.
[148] R. Buick, Carbonaceous Filaments from North-Pole, Western Australia - Are They Fossil Bacteria in Archean Stromatolites - a Reply, Precambrian Research 39 (1988) 311-317.

[149] J.P. Grotzinger and A.H. Knoll, Stromatolites in Precambrian carbonates: Evolutionary mileposts or environmental dipsticks?, Ann. Rev. Earth Planet. Sci. 27 (1999) 313-358.
[150] J. Veizer, Geochemistry of carbonates and related topics: Database, 426 pp., Ruhr University, Bochum, Germany, 1994.
[151] D.Y. Sumner, Carbonate precipitation and oxygen straitfication in Late Archean seawater as deduced from facies and stratigraphy of the Gamohaan and Frisco formations, Transvaal Supergroup, South Africa, Am. J. Sci. 297 (1997) 455-487.
[152] J. Farquhar, H.M. Bao and M. Thiemens, Atmospheric influence of Earth's earliest sulfur cycle, Science 289 (2000) 756-758.
[153] J.P. Greenwood, S.J. Mojzsis and C.D. Coath, Sulfur isotopic compositions of individual sulfides in Martian meteorites ALH84001 and Nakhla: implications for crust-regolith exchange on Mars, Earth Planet. Sci. Lett. 184 (2000) 23-35.
[154] R. Rye, P.H. Kuo and H.D. Holland, Atmospheric carbon-dioxide concentrations before 2.2-billion years ago, Nature 378 (1995) 603-605.
[155] Y.L. Yung and W.B. DeMore, Photochemistry of Planetary Atmospheres, Oxford University Press, 1999.
[156] H. Nair, M. Allen, A.D. Anbar, Y.L. Yung and R.T. Clancy, A Photochemical Model of the Martian Atmosphere, Icarus 111 (1994) 124-150.
[157] J.L. Fox, Upper limits to the outflow of ions at Mars: Implications for atmospheric evolution, Geophys. Res. Lett. 24 (1997) 2901-2904.
[158] K.S. Hutchins, B.M. Jakosky and J.G. Luhmann, Impact of a paleomagnetic field on sputtering loss of Martian atmospheric argon and neon, J. Geophys. Res. 102 (1997) 9183-9189.
[159] B.M. Jakosky and R.J. Phillips, Mars' volatile and climate history, Nature 412 (2001) 237-244.
[160] T. Owen, The composition and early history of the atmosphere of Mars, in: Mars, H.H. Kieffer, B.M. Jakosky, C.W. Snyder and M.S. Matthews, eds., pp. 818-834, The University of Arizona Press, Tucson, 1992.
[161] A.A. Pavlov, L.L. Brown and J.F. Kasting, UV shielding of NH_3 and O_2 by organic hazes in the Archean atmosphere, J. Geophys. Res 106 (2001) 23267-23287.
[162] S.-B.R. Chang and J.L. Kirschvink, Magnetofossils, the magnetization of sediments, and the evolution of magnetite biomineralization, Ann. Rev. Earth Planet. Sci. 17 (1989) 169-195.